catalysts

MDPI

Article

Kinetic Modeling and Quantum Yields: Hydrogen Production via Pd-TiO_2 Photocatalytic Water Splitting under Near-UV and Visible Light

Bianca Rusinque, Salvador Escobedo and Hugo de Lasa *

Chemical Reactor Engineering Centre (CREC), Faculty of Engineering, Western University, London, ON N6A 5B9, Canada; brusinqu@uwo.ca (B.R.); sescobe@uwo.ca (S.E.)
* Correspondence: hdelasa@uwo.ca; Tel.: +1-519-661-2149

Abstract: A palladium (Pd) doped mesoporous titanium dioxide (TiO_2) photocatalyst was used to produce hydrogen (H_2) via water splitting under both near-UV and visible light. Experiments were carried out in the Photo-CREC Water-II Reactor (PCW-II) using a 0.25 wt% Pd-TiO_2 photocatalyst, initial pH = 4 and 2.0 *v*/*v*% ethanol, as an organic scavenger. After 6 h of near-UV irradiation, this photocatalyst yielded 113 cm^3 STP of hydrogen (H_2). Furthermore, after 1 h of near-UV photoreduction followed by 5 h of visible light, the 0.25 wt% Pd-TiO_2 photocatalyst yielded 5.25 cm^3 STP of H_2. The same photocatalyst, photoreduced for 24 h under near-UV and subsequently exposed to 5 h of visible light, yielded 29 cm^3 STP of H_2. It was observed that the promoted redox reactions led to the production of hydrogen and by-products such as methane, ethane, ethylene, acetaldehyde, carbon monoxide, carbon dioxide and hydrogen peroxide. These redox reactions could be modeled using an "*in series-parallel*" reaction network and Langmuir Hinshelwood based kinetics. The proposed rate equations were validated using statistical analysis for the experimental data and calculated kinetic parameters. Furthermore, Quantum yields ($QY_{H^\bullet}$%) based on the $H^\bullet$ produced were also established at promising levels: (a) 34.8% under near-UV light and 1.00 g L^{-1} photocatalyst concentration; (b) 8.8% under visible light and 0.15 g L^{-1}. photocatalyst concentration following 24 h of near-UV.

Keywords: palladium; TiO_2; hydrogen production; visible light; near-UV light; photocatalysis; Photo-CREC Water-II Reactor; kinetic modeling

check for updates

Citation: Rusinque, B.; Escobedo, S.; de Lasa, H. Kinetic Modeling and Quantum Yields: Hydrogen Production via Pd-TiO_2 Photocatalytic Water Splitting under Near-UV and Visible Light. *Catalysts* **2022**, *12*, 113. https://doi.org/10.3390/catal12020113

Academic Editor: Detlef W. Bahnemann

Received: 30 December 2021
Accepted: 12 January 2022
Published: 18 January 2022

Publisher's Note: MDPI stays neutral with regard to jurisdictional claims in published maps and institutional affiliations.

Copyright: © 2022 by the authors. Licensee MDPI, Basel, Switzerland. This article is an open access article distributed under the terms and conditions of the Creative Commons Attribution (CC BY) license (https://creativecommons.org/licenses/by/4.0/).

1. Introduction

The world community is actively researching the production of environmentally friendly energy sources [1]. Hydrogen has attracted the attention of the scientific community due to its great value as an energy carrier with net-zero CO_2 emissions when burned. Hydrogen can be produced by using water and sunlight as primary sources via photocatalytic water splitting [2]. The water splitting reaction takes place at room temperature and close to atmospheric pressure and requires a titanium dioxide (TiO_2) based photocatalyst.

A mesoporous TiO_2 photocatalyst appears to display intrinsic advantages such as: (a) a large surface area with adequate pore sizes; (b) high light absorption; and (c) good electron and chemical species transport properties [3,4]. TiO_2 can be found in three allotropic phases: anatase, rutile and brookite, with anatase being the most photoactive phase. TiO_2 has been proven to be stable, resistant to corrosion, environmentally friendly, largely available in nature and inexpensive [5,6]. However, the main limitation of the TiO_2 photocatalyst for hydrogen production is its wide band gap (c.a., 3.0 eV). Due to this, only 5% of the solar spectrum can be used to activate titanium dioxide. Therefore, the use of sunlight as a source of energy in photocatalysis for hydrogen production leads to a low-efficiency process requiring additional improvements [7,8].

Given these facts, research is required to develop modified photocatalysts for water splitting, with these photocatalysts meeting the following criteria: (a) narrow band gaps

to absorb visible light; (b) chemical stability under redox conditions; (c) inexpensiveness; (d) reusability; (e) hazard-free; and (f) suitability for large-scale hydrogen production [9,10].

To improve photocatalyst efficiency, surface modification by either using soft templates or by doping with a noble metal can be considered. The doping of photocatalysts with metals can narrow the band gaps and improve the optoelectronic semiconductor properties [11]. The photoexcitation of these metals leads to the generation of charge carriers and creates extra photocatalytic active sites, which act as electron collectors and, as a result, facilitate the water splitting process.

Palladium, specifically, has a lower Fermi level compared to TiO_2. When used as a co-photocatalyst, it leads to an effective transfer of electrons to metal sites, reducing the electron/hole recombination and promoting enhanced photocatalytic activity [12]. Additionally, its uniformly irradiated outer particle surface area helps to restrict species diffusional transport limitations [13].

Organic molecules or sacrificial agents perform as electron donors, decreasing electron/hole recombination [14]. Ethanol, for example, is used as an organic scavenger at low concentrations. This scavenger can be easily obtained from renewable sources while being widely available and inexpensive [15].

For economically viable hydrogen production, unique photocatalytic reactor designs are required. These units should have the following characteristics: (a) uniform axial irradiation distribution; (b) must allow for photocatalytic reactions free of species diffusive transport limitations; (c) uniform photocatalyst distribution; (d) high surface/volume reactor ratio; (e) minimum photocatalyst fouling; (f) well-mixed photocatalyst suspension; (g) low-pressure drop; (h) low near-UV and visible light transmittance across unit walls; (i) be corrosion-free to the chemicals used (e.g., ethanol); and (j) have a pH in the 2 to 10 range [16]. The Photo-CREC Water-II Reactor (PCW-II Reactor), designed and developed at the Chemical Reactor Engineering Center (CREC)-UWO in London, Ontario, Canada, meets these various design conditions, required to successfully produce hydrogen via water splitting [16].

In the present study, runs were developed in the PCW-II Reactor using a pH = 4, 2.0 v/v% ethanol and a 0.25 wt% Pd-TiO_2 at 0.15–1.0 gL^{-1} photocatalyst slurry concentrations. Hydrogen and redox by-products such as CO_2, ethane, acetaldehyde and hydrogen peroxide were formed. This led to the establishment of an "*in series-parallel*" reaction network. Product formation rates were based on Langmuir–Hinshelwood (L–M) models, which included adsorbed chemical species at equilibrium. On this basis, the hydrogen and by-product formation rates, with their kinetic parameters, were calculated.

2. Proposed Reaction Mechanism for the "*In Series-Parallel*" Kinetic Reaction Network

Photocatalytic water splitting reactions using Pd-TiO_2 and ethanol as an organic scavenger led to hydrogen formation, as well as to several by-products such as methane, ethane, ethylene, acetaldehyde, CO, CO_2 and hydrogen peroxide (refer to Figure 1). The steps involved in the photocatalytic water splitting reactions can be described as follows:

(a) Photons from a light energy source, whether it be from a visible or near-UV light lamp, reach the photocatalyst outer surface.
(b) Photons with an energy content higher than the semiconductor band gap promote the motion of electrons from the valence band (VB) to the conduction band (CB), creating oxidation sites.
(c) Formed sites diffuse onto the TiO_2 inner surface, reacting with the adsorbed water and producing hydroxyl radicals ($OH^{\bullet}$).
(d) $OH^{\bullet}$ radicals oxidize the adsorbed organic molecules and/or scavenger (ethanol), forming carbon-containing products.
(e) Electrons moving on the TiO_2 inner and outer surfaces are captured by the palladium sites.

(f) Electrons captured in the Pd sites interact with the formed hydrogen protons (H^+) from water, yielding $H^\bullet$ radicals. These $H^\bullet$ radicals dimerize, forming molecular hydrogen.
(g) Formed $OH^\bullet$ radicals couple with each other, forming hydrogen peroxide.

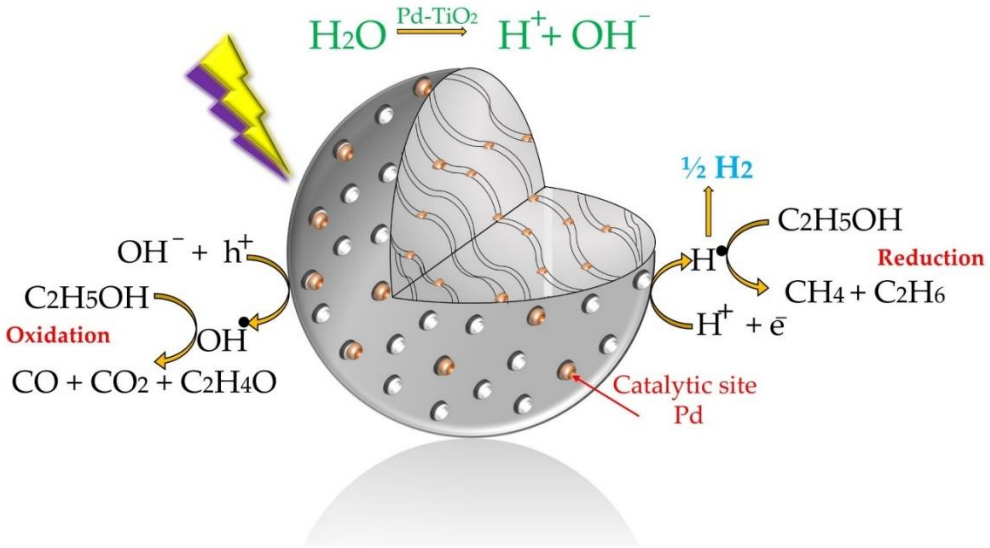


Figure 1. Schematic description of hydrogen formation reaction steps using Pd-TiO_2 as a photocatalyst and ethanol as a scavenger.

An "*in series-parallel*" reaction network was proposed in this research, based on 165 experimental runs, using different photocatalysts concentrations (0.15–1.00 g L^{-1}), as well as various Pd loadings (0.25 wt% to 5.0 wt% Pd) on TiO_2. The proposed network was specifically established for the best performing 0.25 wt% Pd-TiO_2 photocatalyst. It was observed that the 0.25 wt% Pd-TiO_2 photocatalyst yielded a significantly reduced 2.51 eV band gap when compared to the 2.99 eV band gap obtained for undoped mesoporous TiO_2. The absorbed radiation was evaluated via macroscopic irradiation energy balances (MIEB) [17].

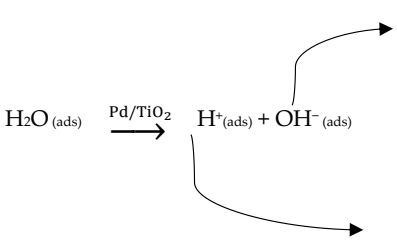
Hydrogen production and carbon-containing product formation proceeded via an "*in series-parallel*" redox reaction network with the following steps:

(a) Step 1: Water dissociates in the presence of TiO_2 and photons, forming $OH^\bullet$ and $H^\bullet$ radicals. Coupled $H^\bullet$ radicals yield molecular hydrogen, as described in Equations (2) and (3).
(b) Step 2: $OH^\bullet$ radicals consume ethanol, which is the sacrificial agent and electron donor. Oxidation byproducts, such as acetaldehyde, CO, CO_2 and hydrogen peroxide [Equations (4)–(8)] form as a result. This contributes to a pH increase, as described in Equation (9).
(c) Step 3: Formed $H^\bullet$ radicals reduce ethanol forming methane and ethane species [Equations (10) and (11)].

2.1. Step 1: $H^\bullet$, $OH^\bullet$ and H_2 Formation

See

$$\mathrm{hv} \overset{\mathrm{Pd/TiO_2\ and\ Photon}}{\rightarrow} h^+ + e^- \quad (1)$$



$$OH^- + h^+ \xrightarrow[Pd/TiO_2]{k_1} OH^\bullet \quad (2)$$

$$H^+_{(ads)} + e^- \xrightarrow[Pd/TiO_2]{k_9} H^\bullet \xrightarrow[Pd/TiO_2]{k_{10}} {}^1/_2\, H_{2\,(g)} \quad (3)$$

2.2. Step 2: $OH^\bullet$ Promoted Reactions

(a) Acetaldehyde

$$C_2H_5OH + OH^\bullet \xrightarrow{Pd/TiO_2} C_2H_5O^- + H_2O \quad (4)$$

$$C_2H_5O^- + OH^\bullet \xrightarrow{Pd/TiO_2} C_2H_4O + H_2O \quad (5)$$

The addition of Equations (4) and (5) yields the following overall equation:

$$C_2H_5OH + 2OH^\bullet \xrightarrow[Pd/TiO_2]{k_2} C_2H_4O + 2H_2O \quad (6)$$

(b) Carbon Dioxide

$$C_2H_5OH + 12OH^\bullet \xrightarrow[Pd/TiO_2]{k_3} 2CO_2 + 9H_2O \quad (7)$$

(c) Hydrogen Peroxide

$$OH^\bullet + OH^\bullet \xrightarrow[Pd/TiO_2]{k_4} H_2O_2 \quad (8)$$

(d) pH variation

$$OH^\bullet \xrightarrow[Pd/TiO_2]{k_5} e^- + OH^- \quad (9)$$

2.3. Step 3: $H^\bullet$ Promoted Reactions

(e) Methane

$$C_2H_5OH + 4H^\bullet \xrightarrow[Pd/TiO_2]{k_6} 2CH_4 + H_2O \quad (10)$$

(f) Ethane

$$C_2H_5OH + 2H^\bullet \xrightarrow[Pd/TiO_2]{k_7} C_2H_6 + H_2O \quad (11)$$

(g) Ethylene

$$C_2H_5OH \xrightarrow[Pd/TiO_2]{k_8} C_2H_4 + H_2O \quad (12)$$

3. Results and Discussion

3.1. Photocatalytic Hydrogen Production under Near-UV Light

The performance of the Pd-TiO_2 photocatalyst was evaluated in the PCW-II Reactor, with a 2.0 v/v% of ethanol—used as a scavenger—with an initial pH adjusted to 4 ± 0.05 and a photocatalyst concentration of 0.15 g L^{-1}. Palladium was used as a TiO_2 co-catalyst, given that Pd enhanced hydrogen production when compared to the undoped mesoporous TiO_2. Pd metal crystallites reduced the band gap and facilitated electron capture [18].

It was found that water splitting under an argon atmosphere and using ethanol as an $OH^\bullet$ scavenger promoted the formation of hydrogen, as well as other chemical species such as methane, ethane, ethylene, acetaldehyde, CO, CO_2, and hydrogen peroxide.

Figure 2 reports the hydrogen formed during six hours of near-UV irradiation when using a 0.25 wt% Pd on TiO_2 and a 0.15 g L^{-1} photocatalyst concentration at an initial

pH = 4 ± 0.05, yielding a maximum hydrogen volume of 113 cm^3 at STP. This volume is three times the volume of hydrogen obtained with undoped mesoporous TiO_2.

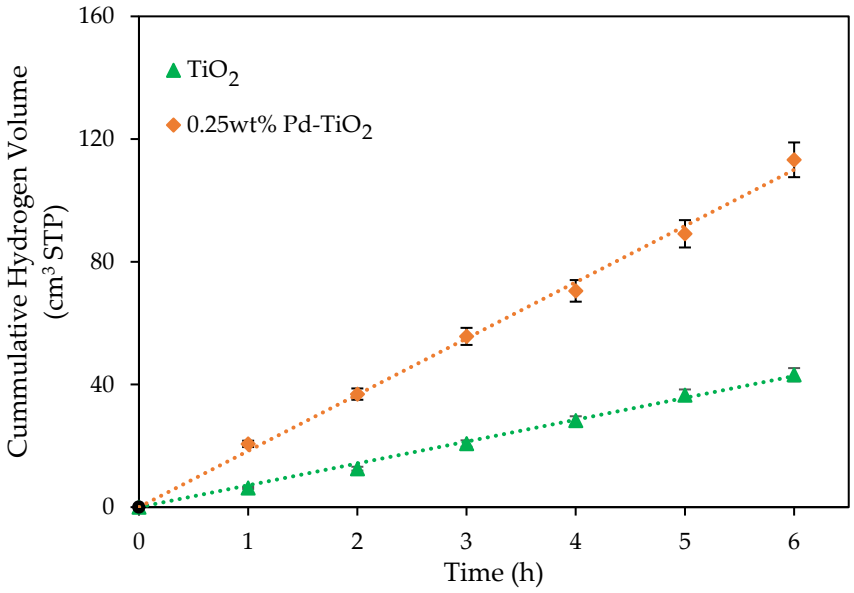


Figure 2. Cumulative hydrogen volumes produced using an undoped TiO_2 photocatalyst and a 0.25 wt% Pd-TiO_2 photocatalyst. Conditions: 0.15 g L^{-1} photocatalyst concentration; 2.0 v/v% ethanol; initial pH = 4 ± 0.05; 6 h under near-UV light. Note: at least three repeats were performed per experiment.

Figure 2 reports that both the undoped TiO_2 and the 0.25 wt% Pd-TiO_2 display a linear hydrogen formation trend during the entire near-UV irradiation period. This is equivalent to zero-reaction order kinetics and represents a stable photocatalytic hydrogen production with no observable photocatalyst deactivation.

Additional experiments were carried out using the 0.25 wt% Pd on TiO_2 at a 1.00 g L^{-1} concentration to determine the photocatalyst concentration influence on hydrogen formation. The results were as described in Figure 3, with higher TiO_2 photocatalyst concentrations leading to higher hydrogen formation rates.

Figure 3 reports that hydrogen production augments by 74% when using a 1.00 g L^{-1} TiO_2 concentration of 0.25 wt% Pd-TiO_2, as compared to undoped TiO_2. In addition, hydrogen production increases by 32% when using a 1.00 g L^{-1} TiO_2 concentration of a 0.25 wt% Pd-TiO_2 photocatalyst compared to the hydrogen obtained with a 0.15 g L^{-1} TiO_2 concentration of 0.25 wt% Pd-TiO_2. Thus, the formed hydrogen augments 1.5 times when the photocatalyst concentration increases approximately seven (7) times, from 0.15 to 1.00 g L^{-1}. Given these results, the photocatalyst performance increase with the higher 1.00 g L^{-1} catalyst concentration was considered moderate, and the 0.15 g L^{-1} concentration was used in further experiments.

3.2. Photocatalytic Hydrogen Production under Visible Light

During the photocatalyst synthesis, palladium was present in a metallic state. However, it was oxidized later during the photocatalyst precursor calcination step. Therefore, a special and additional photocatalyst pretreatment step was implemented in the present study to ensure that most of the palladium was reduced to metallic palladium (Pd^0) prior to hydrogen formation photocatalytic runs. The metallic state of Pd promoted a high photocatalytic activity of the TiO_2 by trapping and storing the photogenerated electrons, thus reducing the rate of the electron-hole recombination [19].

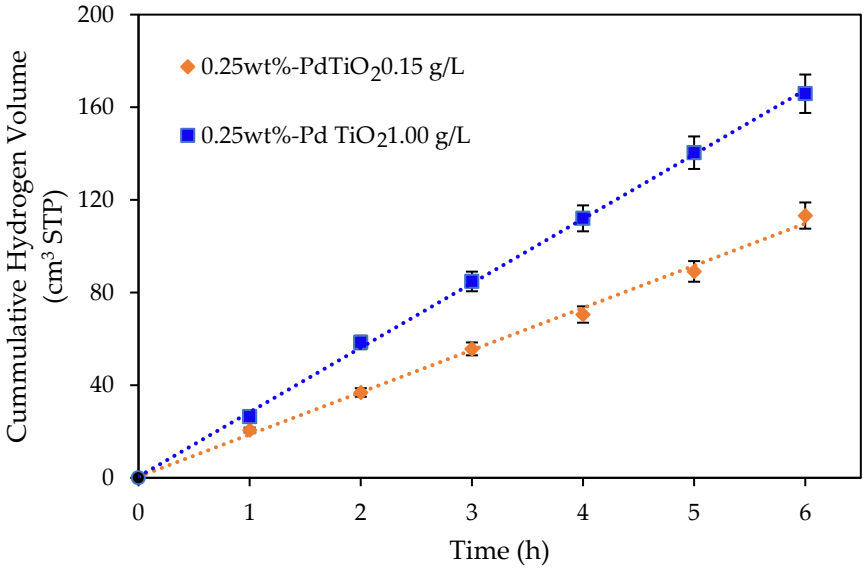


Figure 3. Cumulative hydrogen production using an undoped TiO_2 and a 0.25 wt% Pd-TiO_2 at catalyst concentrations of 0.15 and 1.00 g L^{-1}. Conditions: 2.0 v/v% ethanol, initial pH = 4 ± 0.05 and 6 h under near-UV light. Note: at least three repeats per experiment were performed.

To accomplish this, the prepared Pd-TiO_2 photocatalyst was studied in the PCW-II reactor as follows: (a) 1-h of near-UV photoreduction using a 15 W BLB UV-Lamp; (b) 5 h of visible light employing a 15 W fluorescent visible light lamp.

Figure 4 reports the cumulative hydrogen production with the 0.25 wt% Pd-TiO_2 in the PCW-II Reactor after 1 h of photocatalyst photoreduction under near-UV light, followed by 5 h of visible light [20].

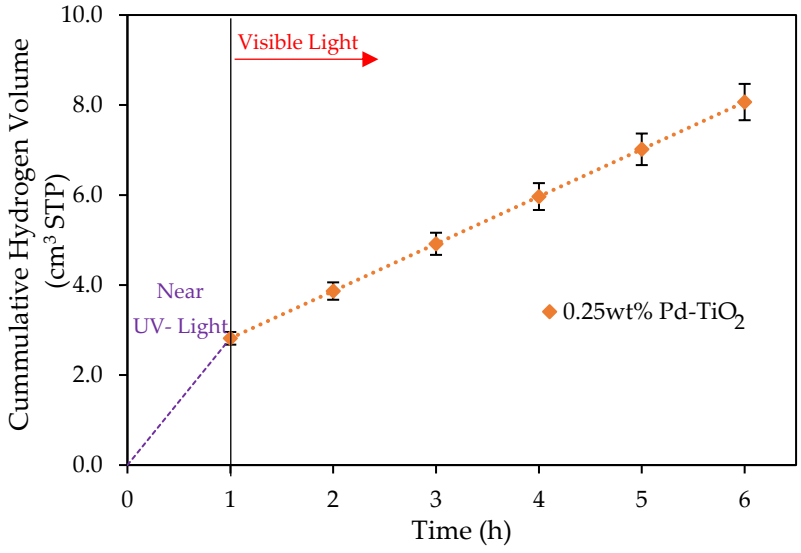


Figure 4. Cumulative formed hydrogen using 0.25 wt% Pd-TiO_2 and a 0.15 g L^{-1} photocatalyst concentration. Conditions: 1 h near-UV light photoreduction; 5 h of visible light; 2.0 v/v% ethanol; initial pH = 4 ± 0.05. Note: at least three repeats per experiment were performed.

Figure 5 reports the volumes of formed hydrogen after 1 h and 24 h of near-UV photoreduction pretreatment, followed by 5 h of visible light irradiation, using the 0.25 wt% Pd-TiO_2 photocatalyst.

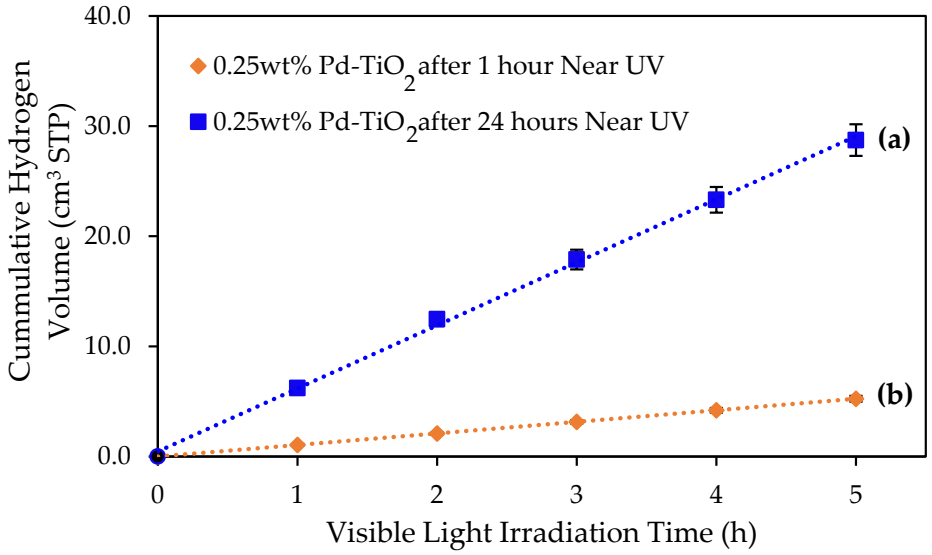


Figure 5. Comparative cumulative hydrogen volume obtained during 5 h of visible light irradiation using the 0.25 wt% Pd-TiO_2 photoreduced photocatalyst as follows: (a) hydrogen volume under visible light after 24 h of near-UV exposure; (b) hydrogen volume under visible light after 1 h of near-UV exposure. Photocatalyst conditions: 0.15 g L^{-1} photocatalyst concentration; 2.0 v/v% ethanol; and initial pH = 4 ± 0.05. Notes: There were at least three repeats per experiment.

The photocatalyst yielded during the visible light irradiation period, 5.25 cm^3 STP hydrogen. The 5.25 cm^3 STP of formed H_2 is 4 times larger than the hydrogen obtained with undoped TiO_2 and 1.7 times greater than the hydrogen produced with the non-photoreduced 0.25 wt% Pd-TiO_2, as reported by Rusinque et al. [21]. Results reported in Figure 5 for the 1 h photoreduced 0.25 wt% Pd-TiO_2 are in line with the XPS analysis, which shows an 81.3% reduction of PdO to Pd^0. Furthermore, for the 0.25 wt% Pd-TiO_2 photocatalyst with 24 h of near-UV photoreduction pretreatment, a cumulative hydrogen volume of 29 cm^3 STP was obtained, with this being consistent with a close to 100% reduction of PdO to Pd^0, as confirmed with XPS.

3.3. Kinetic Modeling

The proposed kinetic model, as given by Equations (2)–(12), is based on the following assumptions [22]:

(a) Reactions take place on the photocatalyst surface.
(b) Reactions are elementary.
(c) Adsorbed chemical species are in equilibrium with those in the bulk solution.
(d) The concentration of water on the photocatalyst surface is constant.
(e) The rate of electron-hole formation is proportional to the local volumetric rate of photon absorption (LVRPA).
(f) The photocatalytic water splitting reactions take place in the PCW-II Reactor, with a 0.25 wt% Pd in TiO_2, a 0.15 g L^{-1} photocatalyst concentration, an initial pH = 4 and 2.0 v/v% ethanol.
(g) Water splits, forming intermediate $OH^•$ and $H^•$ radicals, with $H^•$ reacting further and yielding molecular hydrogen.
(h) Ethanol is consumed as an $OH^•$ organic scavenger via different reaction pathways and forms various oxidation by-products, such as acetaldehyde, CO, and CO_2.
(i) Ethanol and its by-products are reduced via the generated $H^•$ radicals, yielding methane and ethane.

The L–H kinetics can be established in terms of the gas phase species concentrations as follows:

$$r_i = LVRPA\ f\left[\mathrm{H}^+\right] \frac{k_i^I K_i^A C_i}{1 + \sum_{j=1}^{n} K_j^A C_j} = \frac{k_i^* K_i^A C_i}{1 + \sum_{j=1}^{n} K_j^A C_j} \quad (13)$$

where r represents the rate of reaction, $LVRPA$ is the local volumetric rate of photon absorption, f $[H^+]$ denotes the pH influence on the photocatalytic reaction, k_i^* stands for the limiting rate constant of the reaction under the experimental conditions considered (mol $g_{cat}{}^{-1}$ h^{-1}), K represents the equilibrium constant for the adsorption of the chemical species on the photocatalyst (L mol^{-1}) and C_j is the chemical species concentration at any time t (mol L^{-1}).

The k_i^* and K_i^A parameters in Equation (13) are functions of the initial concentration, Co, and the concentration at equilibrium, Ce. These variables can be predicted by simplifying Equation (13) into Equation (14) as follows:

$$r_j \frac{K_j^A C_j}{1 + K_o^A C_o} \quad (14)$$

By using Equation (14), a rate equation can be obtained for each chemical species formed during the photocatalytic water splitting reaction (e.g., hydrogen and by-products). Thus, a set of ordinary differential equations can be established based on the proposed "*in series-parallel*" reaction network.

One of the parameters accounted for in the L–H kinetic model is the equilibrium constant for the adsorption of the chemical species on the photocatalyst. To determine this constant, ethanol adsorption runs were carried out in the PCW-II Reactor under "dark" conditions (no irradiation). Adsorption runs were developed at the same conditions as the ones for the water splitting reactions. First, the reactor was loaded with 6 L of water at different ethanol concentrations (0.5 to 4 v/v%). Following this, 0.15 g L^{-1} of the 0.25 wt% Pd-TiO_2 photocatalyst was added to the solution. The liquid slurry was recirculated for one hour to reach adsorption equilibrium. During this period, a liquid sample was taken every 10 min, and the ethanol concentration in the liquid at equilibrium (Ce) was measured using ultra-fast liquid chromatography (UFLC). Based on the experimental data, the maximum adsorption capacity was given by the following relation:

$$Q_{EtOH} = \frac{Q_{EtOH,max} K_{EtOH}^A C_{EtOH}}{\left(1 + K_{EtOH}^A C_{EtOH}\right)} \quad (15)$$

where Q_{EtOH} is the ethanol solid-phase equilibrium concentration, Ce is the equilibrium concentration in the liquid phase (mol L^{-1}), $Q_{ETOH,max}$ is the maximum solid adsorption capacity (mol $g_{cat}{}^{-1}$) and K is the adsorption constant (L mol^{-1}) [23].

Figure 6 describes the Langmuir chemisorption isotherm obtained ($Q_{EtOH} = Q_{EtOH,max} \cdot K_{EtOH}^A \cdot C_{ETOH} / 1 + K_{EtOH}^A \cdot C_{ETOH}$). It shows that the ethanol adsorption on the 0.25 wt% Pd-TiO_2 is of the chemisorption type. Furthermore, by using a Langmuir linearized equation, as shown in Figure 7, the ethanol adsorption parameters are determined for the 0.25 wt% Pd-TiO_2 photocatalyst. These results are reported in Table 1.

Table 1. Adsorption Constants for Ethanol when Using the 0.25 wt% Pd-TiO_2.

K_{EtOH}^A	$Q_{EtOH,max}$
1.26 mol^{-1} L	0.315 mol^{-1} g_{cat}

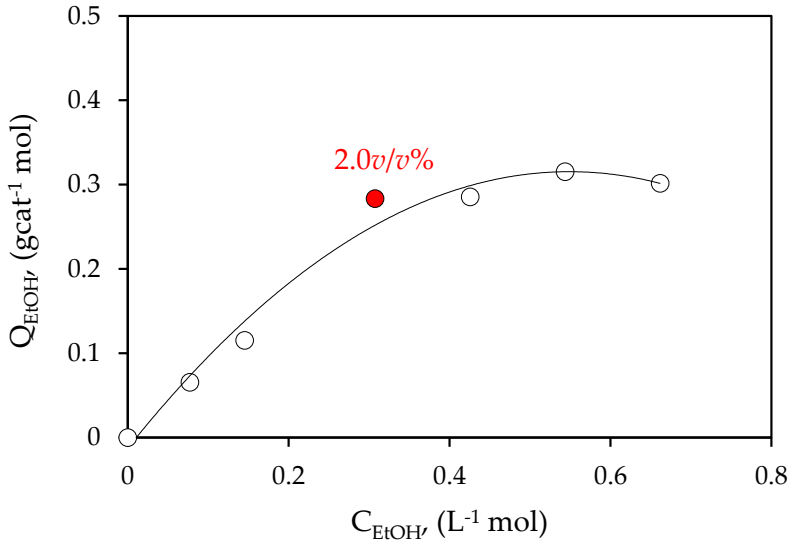


Figure 6. Ethanol adsorbed on 0.25 wt% Pd-TiO_2 photocatalyst.

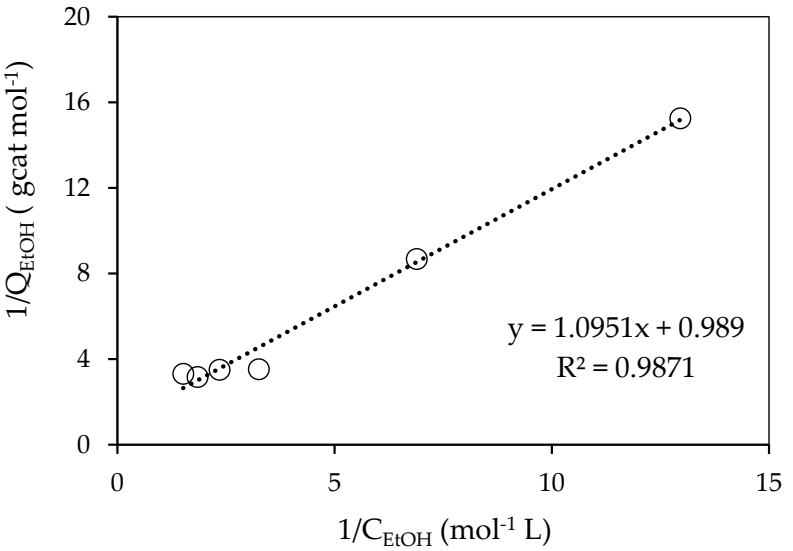


Figure 7. Linearized Langmuir equilibrium isotherm for ethanol on 0.25 wt% Pd-TiO_2.

Outcomes reported in Table 1 differ from those acquired by Escobedo et al. [16,24], who found that ethanol adsorbs on a 1.0wt% Pt-TiO_2 with a $Q_{ETOH,max}$ of 0.163 mol^{-1} g_{cat}. The $Q_{ETOH,max}$ obtained by Escobedo et al. is lower than the $Q_{ETOH,max}$ = 0.315 mol^{-1} g_{cat} found in this research. The $Q_{ETOH,max}$ result from the present study was assigned to the 131 m^2 g^{-1} specific surface area of the Pd-TiO_2 photocatalyst of the present study, with 16–20 nm pores.

The ethanol adsorption isotherm obtained in the present study shows that for ethanol concentrations above 2.0 v/v%, the equilibrium adsorbent-phase concentration remains constant and close to saturation. Therefore, ethanol concentrations surpassing 2.0 v/v% in the photocatalytic water splitting reaction are not justified, given that they do not enhance the hydrogen production rate.

3.4. L–H Equations and the "In Series-Parallel" Reaction Network

The Langmuir–Hinshelwood (L–H) rate-based equations can be used to describe each one of the reaction steps involved in the water splitting reaction. A general expression of the Langmuir–Hinshelwood equation for this system is given by Equation (13).

Furthermore, the species balance for each component "*i*" involved in the photocatalytic water splitting reaction, in the batch PCW-II reactor, can be described by Equation (16):

$$r_i = \frac{1}{W_{irr}}\frac{dN_i}{dt} = \frac{V_L}{W_{irr}}\frac{dN_i/V_L}{dt} = \frac{V_L}{W_{irr}}\frac{dC_i}{dt} \quad (16)$$

where W_{irr} represents the irradiated photocatalyst (g_{cat}), V_L is the reactor liquid slurry volume, N_i stands for the number of *i* moles (mol), *t* denotes the irradiation time (h) and C_i represents the concentration of the chemical species (mol L^{-1}).

Furthermore, by inserting Equation (13) into Equation (16), the concentration changes of the individual chemical species can be described as follows:

$$\frac{dC_i}{dt} = \frac{(W_{irr}/V_L)k_i^* K_i^A C_i}{1 + \sum_{j=1}^{n} K_i^A C_i} \quad (17)$$

Thus, Equation (18) can be obtained from Equation (17) as follows:

$$\frac{dC_i}{dt} = \frac{k_i' K_i^A C_i}{1 + \sum_{j=1}^{n} K_i^A C_i} \quad (18)$$

and:

$$k_i' = \left(\frac{W_{irr}}{V_L}\right) k_i^* \quad (19)$$

with k_i' being the apparent kinetic constant in Equation (19).

Given that the ethanol concentration was significantly higher than those of all other carbon containing by-products, the following inequality was considered:

$$K_{EtOH}^A C_{EtOH} \gg K_{H_2}^A C_{H_2} + K_{CH_4}^A C_{CH_4} + K_{C_2H_6}^A C_{C_2H_6} + K_{C_2H_4}^A C_{C_2H_4} + K_{C_2H_4O}^A C_{C_2H_4O} + K_{CO_2}^A C_{CO_2}$$

Therefore, the ethanol equilibrium sorbent-phase concentration, Q_{EtOH}, can be represented by Equation (20), considering $1 > K_{EtOH}^A C_{EtOH}$:

$$Q_{EtOH} = \frac{Q_{EtOH\ max} K_{EtOH}^A C_{EtOH}}{1 + K_{EtOH}^A C_{EtOH}} \cong Q_{EtOH,max} \quad (20)$$

As a result, at a 2.0 v/v% ethanol concentration, the reaction rate for each chemical species resulting from both water splitting and redox reactions can be expressed as described in Appendix A and as reported in Table 2.

Table 2. Proposed Reaction Rates for the Chemical Species Formed in the Photocatalytic Water Splitting Reaction using Ethanol as an Organic Scavenger.

Chemical Species	Reaction Rate
Acetaldehyde	$r_{C_2H_4O} = k_2' Q_{EtOH,max} = k_2''$
Carbon Dioxide	$r_{CO_2} = k_3' Q_{EtOH,max} = k_3''$
Hydrogen Peroxide	$r_{H_2O_2} = k_4'$
Methane	$r_{CH_4} = k_6' Q_{EtOH,max} = k_6''$
Ethane	$r_{C_2H_6} = k_7' Q_{EtOH,max} = k_7''$
Ethylene	$r_{C_2H_4} = k_8' Q_{EtOH,max} = k_8''$
Hydrogen	$r_{H_2} = k_9'$

3.5. Kinetic Parameters Evaluation

The proposed kinetics of the present study, for hydrogen production (as reported in Table 2), involves 7 reactions and their respective kinetic parameters. These parameters were evaluated using the experimental data obtained utilizing a 0.25 wt% Pd-TiO_2 photocatalyst, 2.0 v/v% ethanol concentration, 0.15 g L^{-1} photocatalyst loading and ini-

tial pH = 4.0 ± 0.05. To accomplish this, minimization of an objective function involving a kinetic model prediction and experimental data was considered, as described in Equation (21).

$$\sum_{i=1}^{n} (V_{i,exp} - V_{i,model})^2 = minimum \quad (21)$$

with $V_{i,exp}$ being the experimentally observed product species volumes at STP conditions, and $V_{i,model}$ being the calculated product species volumes at STP calculated using the proposed kinetics.

Cross-correlation analysis was also developed to establish the numerical interactions between the determined kinetic parameters. Cross-correlation coefficients were, in most cases, much smaller than 1, indicating the small numerical interactions between the determined parameters, as reported by Rusinque [25]. The proposed kinetics and kinetic parameters, as shown later in this manuscript, adequately describe the experimental data, when using near-UV and/or visible light irradiation, for the experimental conditions studied.

3.5.1. Kinetic Parameters under Near-UV Light

Figure 8a–g report a comparison of model predictions and experimental data, using the 0.25 wt% Pd-TiO_2 photocatalyst, 0.15 g L^{-1} photocatalyst concentration, 2.0 v/v% ethanol, initial pH = 4 ± 0.05 and near-UV irradiation.

One significant feature reported in Figure 8a–g is the common linear trend, representing a steady increase of the obtained volumes of all chemical species at STP during the 6 h of irradiation, with no photoactivity decay.

Based on the proposed kinetics and the experimental data, the k_2'', k_3'', k_4', k_6'', k_7'', k_8'' and k_9' intrinsic kinetic rate constants are reported in Table 3, along with their standard deviations and confidence intervals.

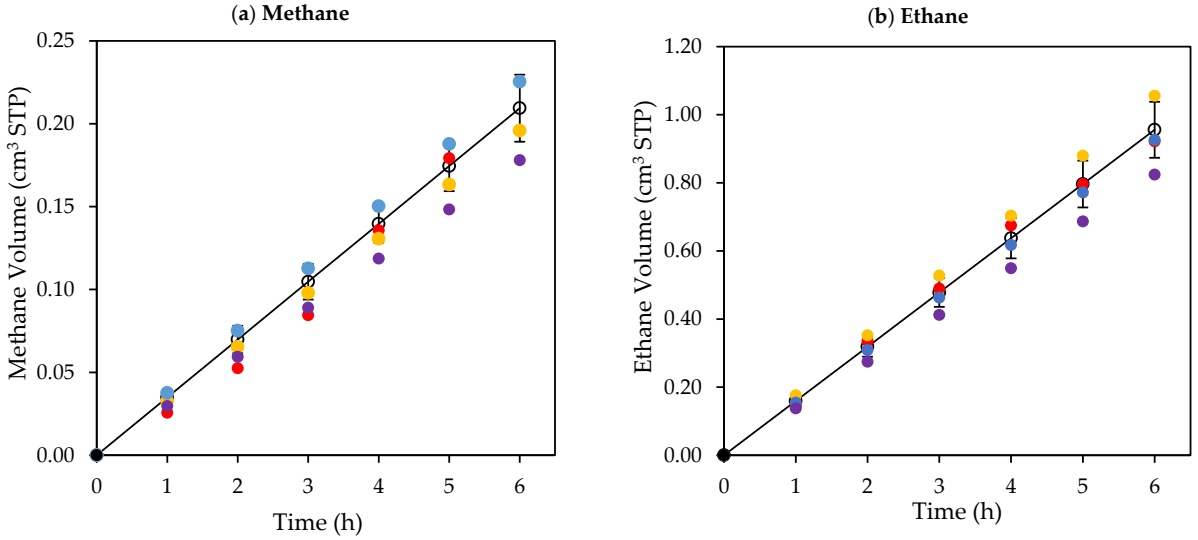


Figure 8. *Cont.*

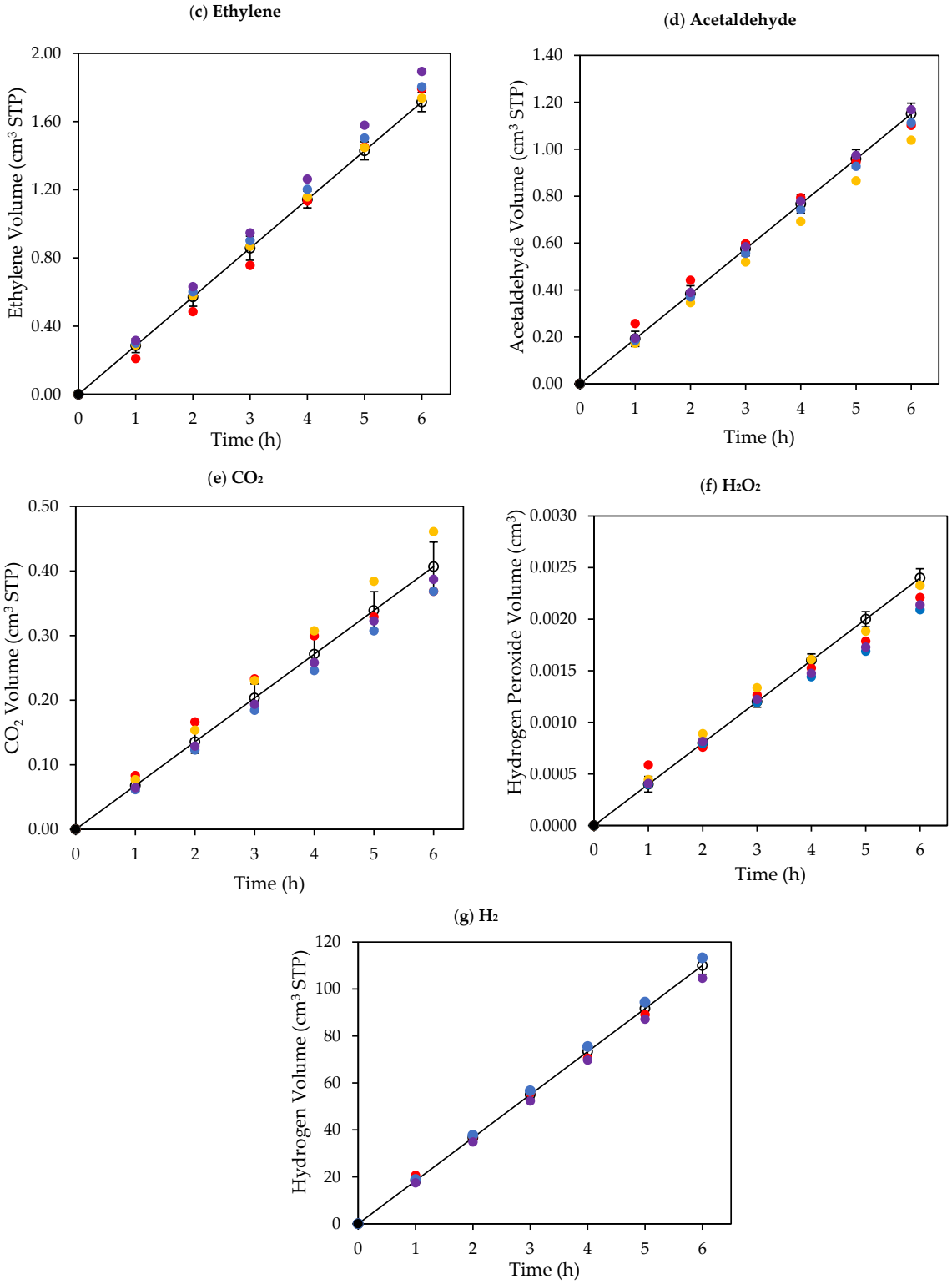


Figure 8. Cumulative chemical species volumes obtained under near-UV: (**a**) methane; (**b**) ethane; (**c**) ethylene; (**d**) acetaldehyde; (**e**) CO_2; (**f**) H_2O_2; and (**g**) H_2. Experimental data are represented by (○) filled with different colors, each color represents a different experimental run, and model predictions are represented with solid lines. Experimental conditions: 0.25 wt% Pd-TiO_2; 0.15 g L^{-1} photocatalyst concentration; initial pH = 4.0 ± 0.05; and 2.0 v/v% ethanol.

Table 3. Intrinsic Kinetic Rate Constants for Hydrogen and By-Products under Near-UV light with 2.0 *v*/*v*% Ethanol. The $Q_{EtOH,\ max}$ adsorption constant for ethanol was set to 0.3 mol g_{cat}^{-1}, as shown in Section 3.3.

	Intrinsic Kinetic Rate Constant (mol g_{cat}^{-1} h^{-1})	STD (±)	Confidence Interval
k_2''	9.09×10^{-6}	3.93×10^{-7}	8.72×10^{-7}
k_3''	3.28×10^{-6}	3.11×10^{-7}	7.23×10^{-7}
k_4'	1.67×10^{-5}	6.89×10^{-7}	1.48×10^{-6}
k_6''	1.71×10^{-6}	1.74×10^{-7}	4.16×10^{-7}
k_7''	7.75×10^{-6}	6.79×10^{-7}	1.52×10^{-6}
k_8''	1.50×10^{-5}	4.61×10^{-7}	9.98×10^{-7}
k_9'	9.10×10^{-4}	2.92×10^{-5}	4.85×10^{-5}

Table 3 shows the calculated intrinsic kinetic rate constants with limited standard deviations. These results point to the adequacy of the intrinsic rate constants under near-UV light. Regarding $k_{1'}$ and $k_{5'}$, they were set to 1.90×10^{-3} mol g_{cat}^{-1} h^{-1} and 3.07×10^{-1} h^{-1} for $OH^{\bullet}$ radical formation and OH^{-} change, respectively. It is recommended to further analyze the validity of these set values in future research studies.

Following the kinetic modeling development, the model was validated using reconciliation plots, as reported in Figure 9. It was confirmed that the proposed kinetics provides a good prediction of all chemical species concentrations.

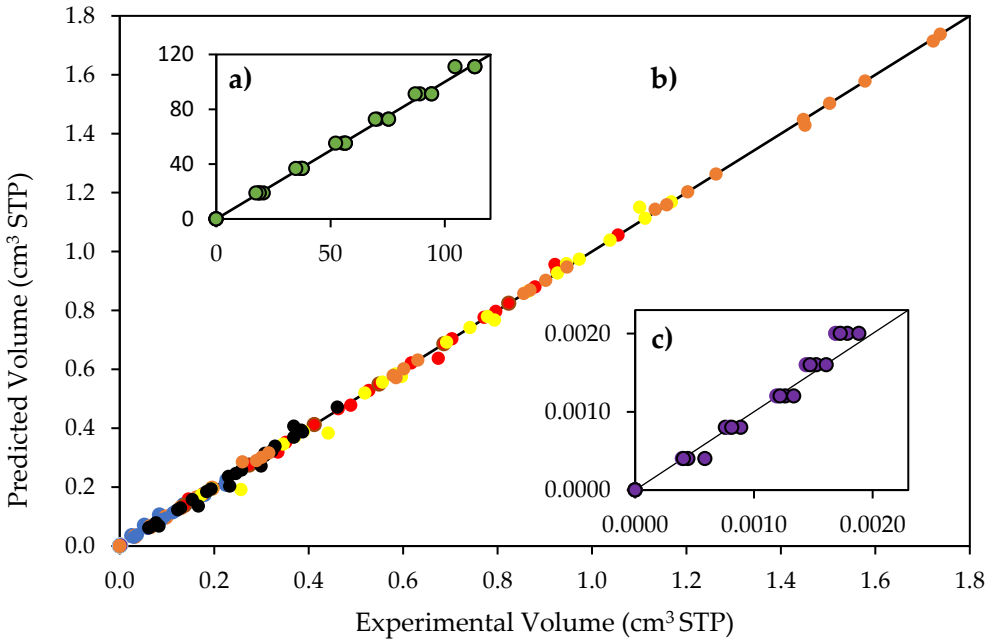


Figure 9. Reconciliation plot for predicted and experimentally observed species volumes. Notes: (**a**) hydrogen volumes: 0 to 113 cm^3 STP; (**b**) CO_2, CH_4, C_2H_4O, C_2H_6 and C_2H_4 volumes, 0 to 1.8 cm^3; and (**c**) hydrogen peroxide volumes, 0 to 0.0022 cm^3 STP. Conditions: 0.25 wt% Pd-TiO_2 photocatalyst; 0.15 g L^{-1} photocatalyst concentration; near-UV light. Experimental error of ±3.4%.

3.5.2. Kinetic Parameters under Visible Light

The adequacy of the "*in series-parallel*" model for water splitting was also evaluated, with the 0.25 wt% Pd-TiO_2 being photoreduced for 1 h with near-UV light, followed by 5 h of visible light irradiation. The selected conditions for the experiments were as follows: 0.15 g L^{-1} photocatalyst; 2.0 *v*/*v*% ethanol; and initial pH of 4.0 ± 0.05. Figure 10 reports the experimental and model predictions, which display a common linear increasing trend in the cumulative formation of hydrogen and various by-products. The hydrogen peroxide

concentration was, however, the exception, yielding a non-linear trend, increasing first, and stabilizing later, as reported in Figure 10f.

Table 4 reports the seven determined intrinsic kinetic constants along with their small standard deviations and 95% confidence intervals. The $k_{1'}$ constant was set to 3.45×10^{-4} mol g_{cat}^{-1} h^{-1}, while the $k_{5'}$constant for the pH increase was set to 9.11×10^{-2} h^{-1}.

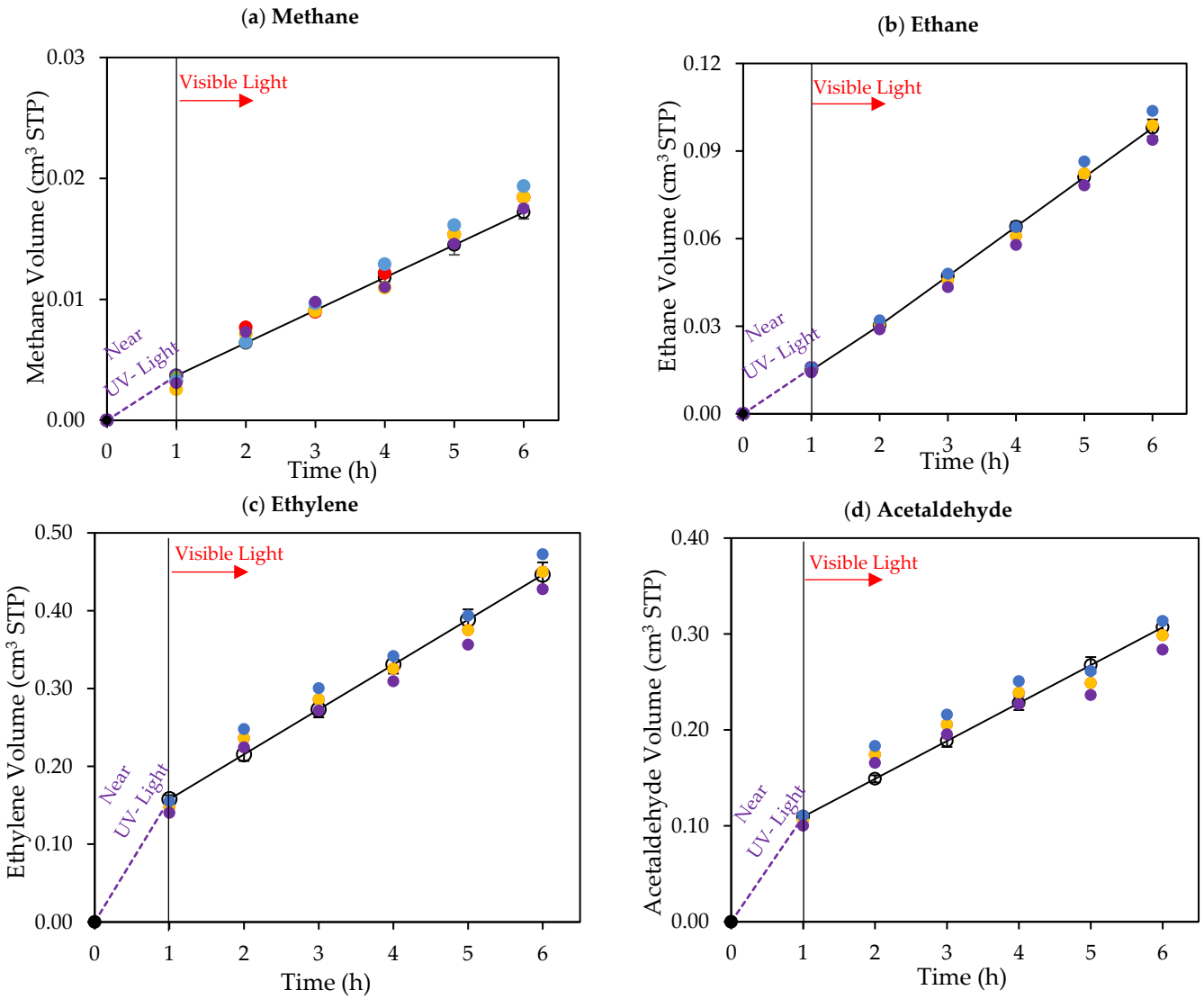


Figure 10. *Cont.*

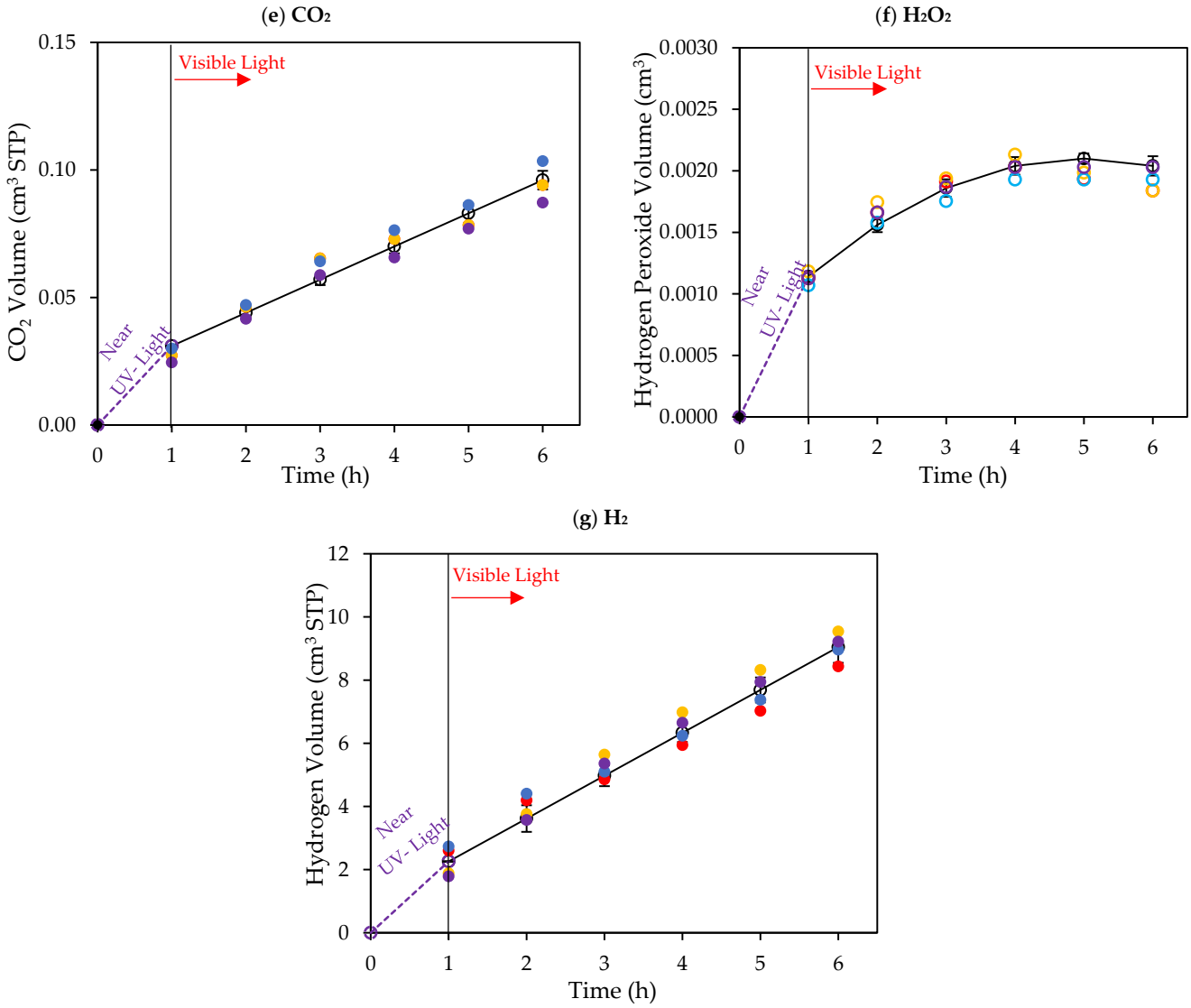


Figure 10. Cumulative chemical species volumes obtained under 1 h of near-UV followed by 5 h of visible light near-UV: (**a**) methane; (**b**) ethane; (**c**) ethylene; (**d**) acetaldehyde; (**e**) CO_2; (**f**) H_2O_2; and (**g**) H_2. Experimental data are represented by (○) filled with different colors, each color represents each experimental run, and model predictions are represented with solid lines. Experimental conditions: 0.25 wt% Pd-TiO_2; 0.15 g L^{-1} photocatalyst concentration; initial pH = 4.0 ± 0.05; and 2.0 v/v% ethanol.

Table 4. Intrinsic Kinetic Rate Constants for Hydrogen Production and By-Product Formation under Visible Light, with 2.0 v/v% Ethanol. Photocatalyst was photoreduced for 1 h under near-UV. The $Q_{EtOH,\,max}$ adsorption constant was set to 0.315 mol $g_{cat}{}^{-1}$, as shown in Section 3.3.

Intrinsic Kinetic Rate Constant (mol $g_{cat}{}^{-1}$ h^{-1})		STD (±)	95% Confidence Interval
k_2''	1.15×10^{-9}	7.03×10^{-11}	2.14×10^{-10}
k_3''	4.98×10^{-9}	3.07×10^{-10}	8.98×10^{-10}
k_4'	3.68×10^{-5}	4.90×10^{-6}	1.01×10^{-5}
k_6''	1.15×10^{-9}	7.03×10^{-11}	2.14×10^{-10}
k_7''	6.53×10^{-9}	2.31×10^{-10}	6.70×10^{-10}
k_8''	2.18×10^{-8}	7.70×10^{-10}	2.15×10^{-9}
k_9'	5.11×10^{-7}	7.01×10^{-8}	1.76×10^{-7}

As in the case of the photocatalyst irradiated with only near-UV light, the adequacy of the established kinetic model was further validated using reconciliation plots, as reported in Figure 11. It was observed that the proposed kinetics provide a good prediction of the experimental data, both hydrogen production and the formation of various by-products, under the visible light irradiation period.

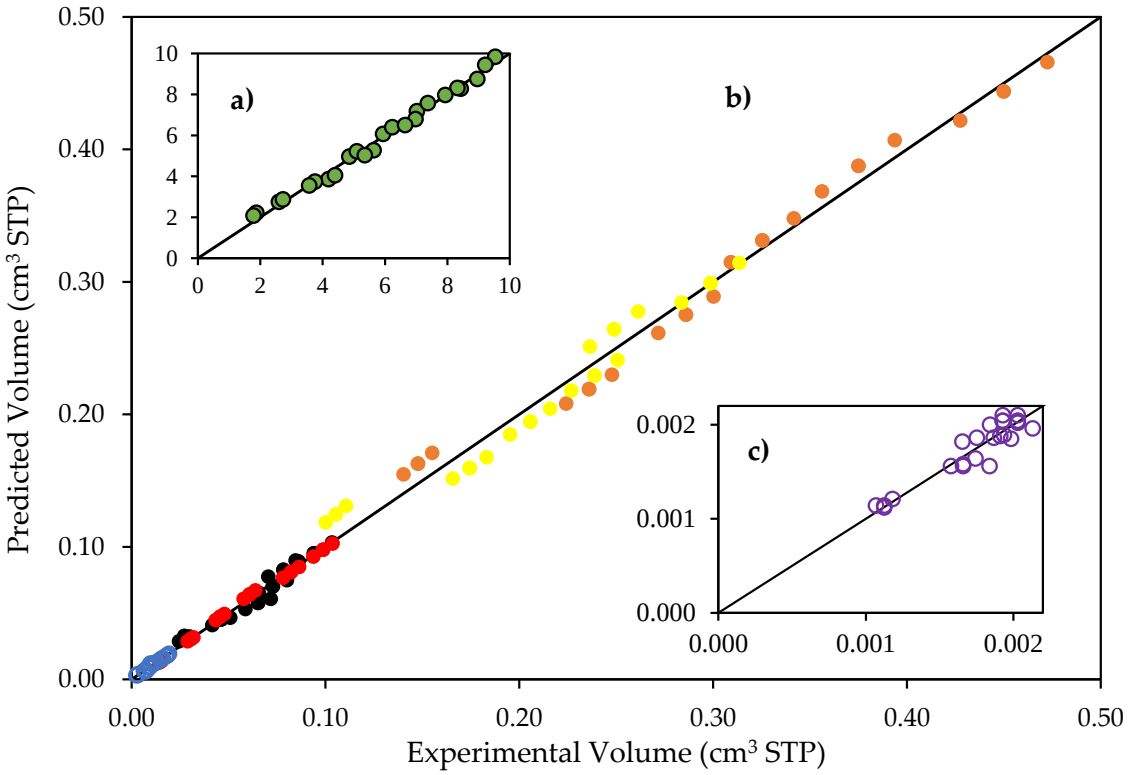


Figure 11. Reconciliation plot for predicted and experimentally observed species volumes. Notes: (**a**) hydrogen volumes, 0 to 10 cm^3 STP; (**b**) CO_2, CH_4, C_2H_4O, C_2H_6 and C_2H_4 volumes, 0 to 0.5 cm^3; and (**c**) hydrogen peroxide volumes, 0 to 0.0022 cm^3 STP. Conditions: 0.25 wt% Pd-TiO_2 photocatalyst. Experimental error of ±5.5%.

3.6. Quantum Yield (QY) Evaluation

The quantum yield is a parameter used to evaluate the photon utilization efficiency in photocatalytic reactors [26]. For hydrogen production, a phenomenologically relevant quantum yield can be defined in terms of the hydrogen radical formation rate over the absorbed photon rate [27]. Therefore, a $QY_{H^\bullet}\%$ can be calculated as follows:

$$QY_{H^\bullet}\% = \left[\frac{\text{moles of } H^\bullet/\text{s}}{\text{moles of photons absorbed by the photocatalyst/s}}\right]100. \quad (22)$$

with $QY_{H^\bullet}\%$ and $QY_{H_2}\%$ being related as follows:

$$QY_{H^\bullet}\% = \left[\frac{\left(\frac{dN_{H^\bullet}}{dt}\right)}{P_a}\right]100 = 2\,QY_{H_{2;}}\,\%\,\% = 2\left[\frac{\left(\frac{dH_2}{dt}\right)}{P_a}\right]100 \quad (23)$$

where $\frac{dN_{H^\bullet}}{dt}$ represents the rate of the moles of hydrogen radicals formed over the photocatalyst absorbed photon rate.

The $QY_{H^\bullet}\%$ calculation requires the absorbed photon rate by the photocatalyst surface (P_a). To determine P_a, Macroscopic Irradiation Energy Balances (MIEB) are required. MIEB

can be established by using a "photocatalyst control volume", established by Salaices, Serrano and de Lasa [28] as follows:

$$P_a = P_i - P_{bs} - P_t \quad (24)$$

where P_a is the rate of absorbed photons, P_i represents the rate of photons reaching the reactor inner surface, P_{bs} stands for the rate of backscattered photons exiting the system and P_t denotes the rate of transmitted photons in Einstein/s. Additional information regarding MIEBs is provided by Rusinque et al. [25].

3.6.1. Evaluation of Quantum Yields under Near-UV Light

The calculated $QY_{H^\bullet}$% for the 0.25 wt% Pd-TiO_2 mesoporous photocatalyst, using a 0.15 g L^{-1} photocatalyst concentration, 2.0 v/v% ethanol, an initial pH = 4 ± 0.05 and near-UV light was determined.

Figure 12 reports a consistent and steady $QY_{H^\bullet}$% over 6 h of near-UV irradiation. During the first hour under near-UV irradiation, the $QY_{H^\bullet}$% reaches a stable value of 13.7%, remaining constant during the following 5 h and showing the stable performance of the 0.25 wt% Pd-TiO_2 photocatalyst. This $QY_{H^\bullet}$% is significantly higher than the 5.0% quantum yield obtained for the undoped TiO_2, at the same experimental conditions. Furthermore, one can notice that this $QY_{H^\bullet}$% improved when compared to the 8% quantum yield reported by Escobedo et al. [29] for DP25 doped with Pt.

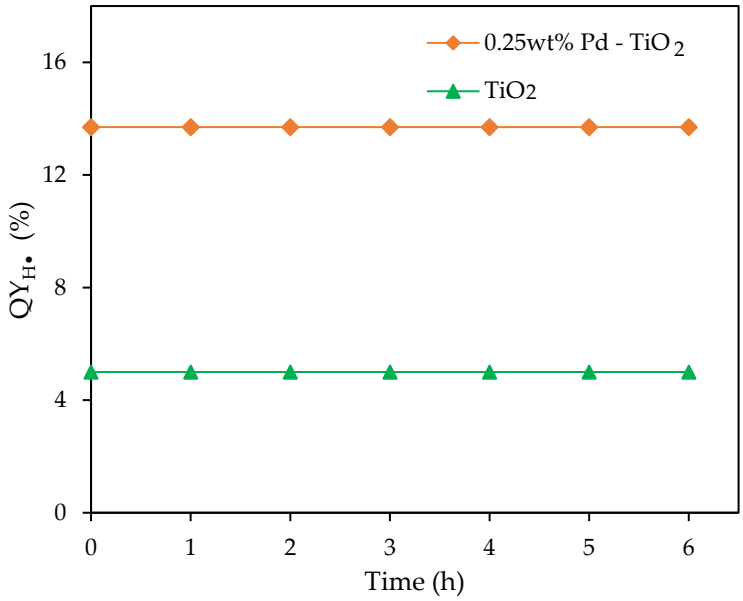


Figure 12. $QY_{H^\bullet}$% for a 0.25 wt% Pd-TiO_2 and for undoped TiO_2 at various irradiation times, under near-UV Light. Conditions: 0.15 g L^{-1} of photocatalyst; initial pH = 4 ± 0.05; 2.0 v/v% ethanol.

Further $QY_{H^\bullet}$% calculations were developed for the 0.25 wt% Pd–TiO_2 at different photocatalyst concentrations. Figure 13 reports the $QY_{H^\bullet}$% obtained by augmenting the photocatalyst concentration from 0.15 g L^{-1} up to 1.00 g L^{-1}. It was observed that there was a consistent increase of the $QY_{H^\bullet}$%, which remained stable during the entire irradiation period, with no noticeable photocatalyst activity decay. A detailed $QY_{H^\bullet}$% calculation is provided in Appendix B.

Thus, using a 0.25 wt% Pd loading on a TiO_2 photocatalyst at 0.15 g L^{-1} and 1.00 g L^{-1} photocatalyst concentrations, and near-UV light, led to a favorable 13.7 $QY_{H^\bullet}$% and to a 34.8 $QY_{H^\bullet}$% respectively.

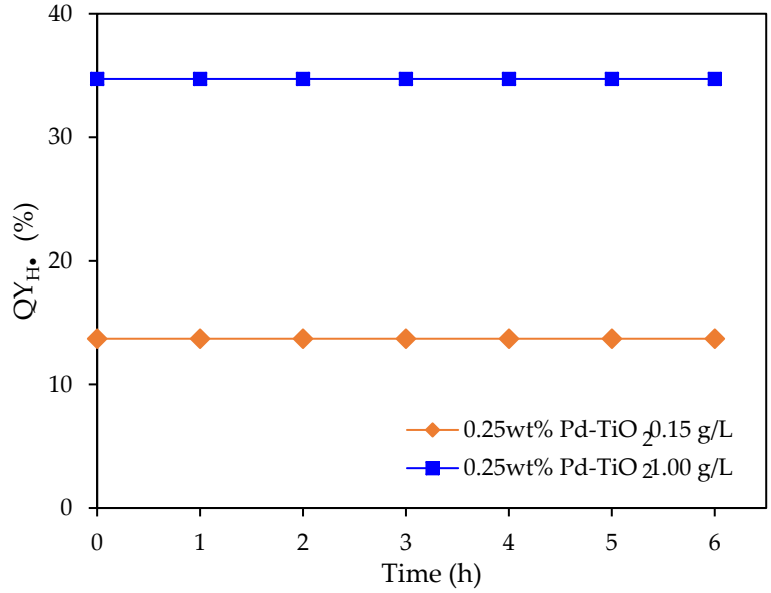


Figure 13. $QY_{H\bullet}$% at various irradiation times under near-UV irradiation using 0.15 and 1.00 g L^{-1} photocatalyst concentrations. Note: 0.25 wt% Pd on TiO_2; 2.0 v/v% ethanol. Initial pH = 4 ± 0.05.

3.6.2. Evaluation of Quantum Yields under Visible Light

The $QY_{H\bullet}$% for the mesoporous photocatalyst, doped with palladium (0.25%wt Pd-TiO_2), was established under the following conditions: (a) photocatalyst slurry concentrations of 0.15 g L^{-1}, (b) 2.0 v/v% ethanol, (c) pH = 4 ± 0.05 and (d) visible light. The $QY_{H\bullet}$% was calculated for the photocatalyst under two different conditions: (1) photocatalyst irradiated with visible light for 6 h, and (2) photocatalyst photoreduced for 1 h first under near-UV light and then irradiated with visible light for the remaining 5 h.

The determined $QY_{H\bullet}$% for the 0.25%wt Pd-TiO_2 under visible light only was 1.13%. This $QY_{H\bullet}$% was moderately higher than the 0.23% obtained for the undoped TiO_2. This rather low $QY_{H\bullet}$% for the Pd-TiO_2 photocatalysts under visible light was attributed to the 49.8 wt% amount of metallic palladium present, as described in Section 4.2.

On the other hand, the $QY_{H\bullet}$% for the 0.25 wt% Pd-TiO_2, photoreduced for 1 h with near-UV light and then irradiated with visible light, was 1.6%. This can be the result of the 81.7 wt% Pd^0 present, after 1 h of near-UV photoreduction, as shown in the photocatalyst characterization section of this paper.

Authors such as Ravishankar [30] reported a calculated quantum yield in the 0.36 to 0.43% range, for palladium loadings between 0.1 and 0.4 wt% under visible light. Thus, the $QY_{H\bullet}$% obtained in the present study were 3–4 times larger than the ones reported by Ravishankar [30].

Figure 14 reports the $QY_{H\bullet}$% for the 1 h near-UV photoreduced photocatalyst, exposed later to visible light. The 1.6% $QY_{H\bullet}$% remains stable during the entire irradiation period, without noticeable photocatalyst deactivation.

3.6.3. Effect of Photoreduction Period on Quantum Yields

Given that the highest $QY_{H\bullet}$% of 1.6% was observed for the 0.25 wt% Pd-TiO_2 photocatalyst under 1 h of near-UV photoreduction, followed by 5 h of visible light irradiation, further $QY_{H\bullet}$% evaluations were developed. To achieve this, the near-UV photocatalyst photoreduction period was extended from 1 h to 24 h.

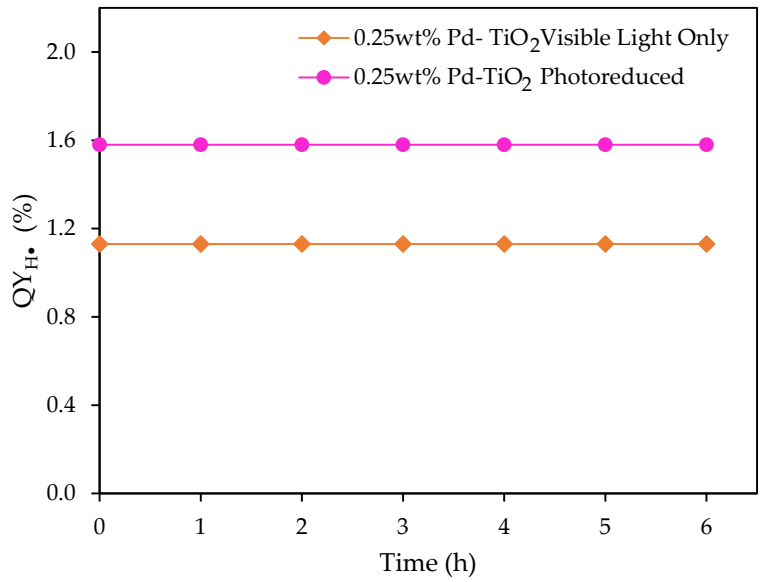


Figure 14. $QY_{H^\bullet}$% for the 0.25 wt% Pd-TiO_2 photocatalyst, at 0.15 g L^{-1} photocatalyst concentration, and various visible light irradiation times. Initial pH = 4 ± 0.05 and 2.0 v/v% ethanol. Note: the photocatalyst reported with the pink line was photoreduced for 1 h under near-UV light, followed by 5 h of visible light irradiation.

Figure 15 and Table 5 report the $QY_{H^\bullet}$% obtained for the 24 h of near-UV photoreduction, followed by 5 h of visible light irradiation. The selected conditions for the reaction remained unchanged, as in previous experimental runs: (a) 2.0 v/v% ethanol; (b) initial pH = 4 ± 0.05; and (c) 0.15 g L^{-1} of TiO_2.

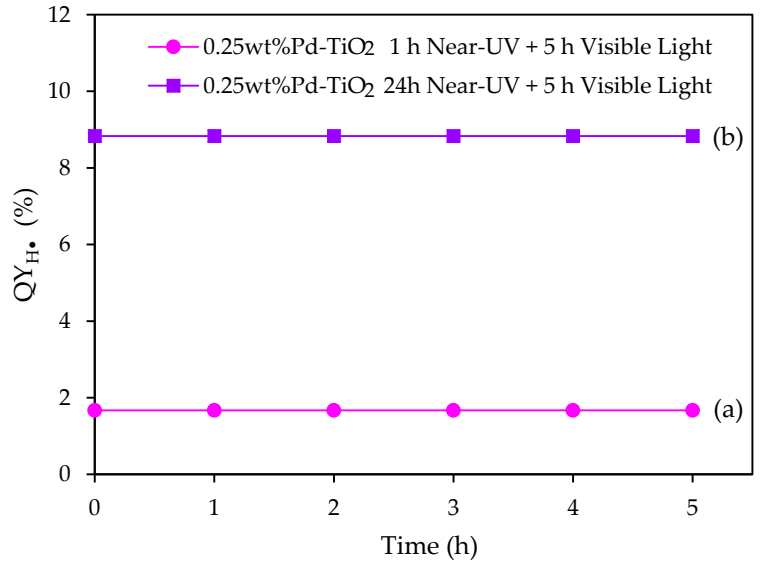


Figure 15. $QY_{H^\bullet}$% at various visible light irradiation times: (a) 1 h of near-UV photoreduction, followed by 5 h of visible light irradiation; and (b) 24 h of near-UV photoreduction, followed by 5 h of visible light irradiation. Note: Conditions: 0.15 g L^{-1} concentration of 0.25 wt% Pd on TiO_2; 2.0 v/v% ethanol; initial pH = 4 ± 0.05.

Table 5. Quantum Yields Using a 0.25%wt Pd-TiO_2 Photocatalyst Based on moles of H_2 and $H^{\bullet}$ at different conditions.

Conditions	$QY_{H_2}\%(\%) = \left[\frac{\left(\frac{dN_{H2}}{dt}\right)}{Pa}\right]100$	$QY_{H^{\bullet}}(\%) = \left[\frac{\left(\frac{dN_{H^{\bullet}}}{dt}\right)}{P_a}\right]100$
• Near-UV irradiation • Photocatalyst concentration: 1.00 g L^{-1} • Ethanol concentration: 2.0 v/v% • Initial pH: 4 ± 0.05	17.4	34.8
• Near-UV irradiation. • Photocatalyst concentration: 0.15 g L^{-1} • Ethanol concentration: 2.0 v/v% • Initial pH: 4 ± 0.05	6.9	13.7
• 5 h of visible light, after 24 h • under near-UV irradiation. • Photocatalyst concentration: 0.15 g L^{-1} • Ethanol concentration: 2.0 v/v% • Initial pH: 4 ± 0.05	4.4	8.8

It was observed that using the extended 24 h near-UV photoreduction rather than the 1 h provided a noticeable increase in the $QY_{H^{\bullet}}$% under visible light, with this reaching 8.80% as described in Figure 15. This $QY_{H^{\bullet}}$% is five times greater than the one for the photocatalyst photoreduced for 1 h under near-UV light. The observed rise in the $QY_{H^{\bullet}}$% was attributed to the almost 100 wt% of the palladium being present as Pd^0, as shown with XPS, and reported in Section 4.2.

Considering the reaction path as per Equations (2) and (3), with one absorbed photon yielding one $H^{\bullet}$ radical, a maximum theoretical $QY_{H^{\bullet}}$% of 100% can be anticipated. The quantum yield for a 0.25%wt Pd-TiO_2 photocatalyst with a concentration of 1.00 g L^{-1} under near-UV light was 34.8%. The quantum yield for a 0.25%wt Pd-TiO_2 photocatalyst with a concentration of 0.15 g L^{-1} irradiated for 24 h under near-UV, followed by visible light irradiation, was 8.8%. Thus, the performance of the photocatalysts of the present study, as quantified using $QY_{H^{\bullet}}$%, can be considered promising.

4. Experimental Methodology

4.1. Photocatalyst Synthesis

The mesoporous photocatalyst was synthesized by a sol–gel method, using evaporation-induced self-assembly (EISA), as shown in Figure 16. For the photocatalyst preparation, the following reagents were used: (a) ethanol USP (C_2H_5OH) obtained from commercial alcohols; (b) hydrochloric acid (HCl, 37% purity); (c) a polymeric soft template (pluronic F-127 ($PEO_{106}PPO_{70}PEO_{106}$); (d) anhydrous citric acid; (e) a titanium precursor (titanium IV isopropoxide); and (f) palladium (II) chloride ($PdCl_2$, 99.9% purity). All the reagents were purchased from Sigma Aldrich (Oakville, ON, Canada).

During the condensation sol–gel photocatalyst synthesis, Pd was present in a metallic state. However, given that the organic template polymer had to be removed before photocatalyst use, a calcination step was implemented. As a result, palladium was oxidised. Thus, following calcination, palladium had to be reduced to Pd^o. To accomplish this, the doping metal was contacted with 1 cm^3/s of Ar/H_2 gas blend (90/10%, Praxair) in a flow reactor at 500 °C for 3 h [16]. Under these conditions, palladium was partially reduced, as shown with the XPS analysis. Therefore, an additional step was implemented to ensure complete palladium reduction. The prepared Pd-TiO_2 was irradiated with a BLB near UV-Lamp in the PCW-II reactor at room temperature for 60 min. More detailed information about the synthesis of the photocatalyst can be found in Rusinque et al. [20].

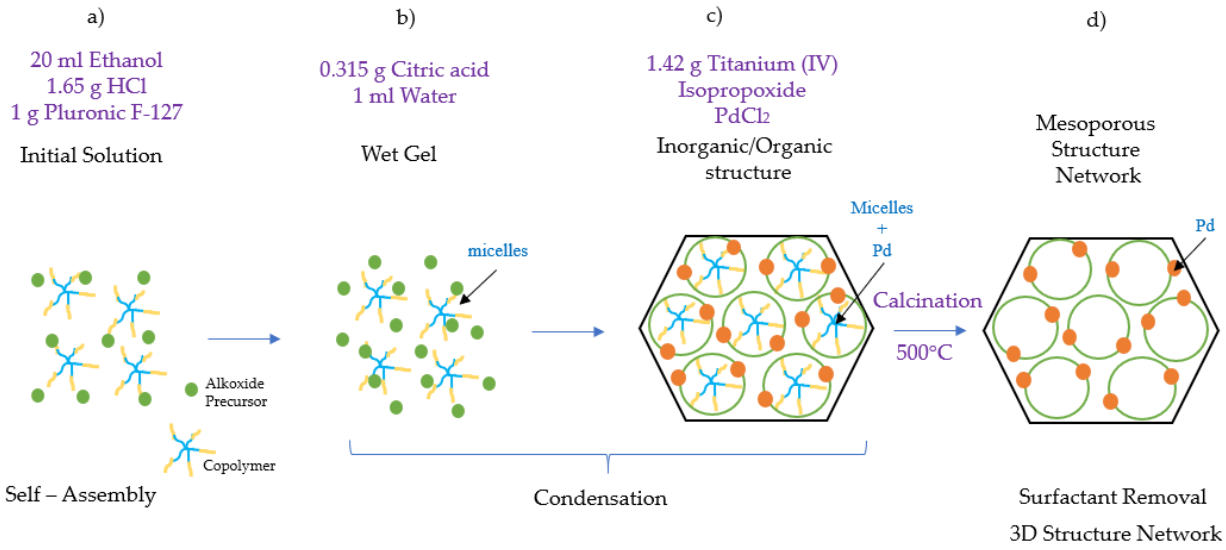


Figure 16. Schematic description of the Pd-TiO_2 photocatalyst synthesis: (**a**) *self-assembly step*, ethanol acts as a hydrophilic compound attaching to the hydrophobic PPO core of the polymer F-127; (**b**) *condensation step*, micelles of the amphiphilic block copolymer are created, (**c**) the PEO tails become attached to the metallic precursor TiO_2, forming a hybrid layer; and (**d**) s*urfactant removal step*, the resultant gel is calcined for 6 h at 500 °C, yielding a well-defined 3D crystalline mesoporous titanium photocatalyst [31–33].

4.2. Photocatalyst Characterization

Various physicochemical techniques were used to assess the photocatalyst Pd-TiO_2 properties, including chemical composition (elemental composition and chemical state), physical properties (surface area, pore size distribution and pore size, phase composition, metal dispersion and metal crystallite size) and band structure (band gap).

The BET (Brunauer–Emmett–Teller) method was employed to establish the 131 $m^2\ g^{-1}$ specific surface area for the 0.25 wt% Pd-TiO_2. Furthermore, by using the Barrett–Joyner–Halenda (BJH) method with an N_2 desorption isotherm, the pore size distribution was found to be unimodal with an average pore size of 16.5 nm.

An H_2 Temperature Programmed Reduction (TPR) of the Pd-TiO_2 photocatalyst was carried out in a AutoChem II Analyzer (Micromeritics, Norcross, GA, U.S.A). The TPR analysis showed that palladium oxide reduction yields four distinctive TPR peaks [34]. The first negative peak, at 68 °C, was attributed to the decomposition of palladium β-hydride. The second broad peak, at 225 °C, was assigned to palladium oxide reduction. The third peak, at 415 °C, was ascribed to the interaction between the Pd species and the TiO_2 support. The fourth one, at 594 °C, was attributed to the reduction of Ti^{+4} ions surface species [35,36].

Pulse Chemisorption allowed one to determine the fraction of metal active species available [37], and hydrogen chemisorption showed a high 75% metal dispersion for the 0.25 wt% Pd-TiO_2.

The minimum TiO_2 crystallite size was determined using the Scherrer Equation and the XRD peak, broadening to be 11 nm for 0.25 wt% Pd-TiO_2. This compared to the 21 nm determined for undoped TiO_2.

A UV–VIS–NIR Spectrophotometer (Shimadzu UV-3600, Nakagyo-ku, Kyoto, Japan) equipped with an integrating sphere was used to determine the band gap. It employed $BaSO_4$ as a reference material [38]. By using the Kubelka–Munk (K–M) method, Tauc plots were developed to establish the corresponding band gap. When using the 0.25 wt% Pd-TiO_2, a linear extrapolation yielded a 2.51 eV band gap, which was a smaller band gap than the 3.2 eV obtained from undoped TiO_2.

Scanning electron microscopy (SEM) (Hitachi SU-8230, Atlanta, GA, USA) provided detailed high-resolution images of the photocatalyst as observed in Appendix C, show-

ing the formation of photocatalyst agglomerates as large as 4 μm with 50 nm average crystallite sizes.

X-ray photoelectron spectroscopy (XPS) (Kratos AXIS Supra, Manchester, U.K) analysis was used to establish the elemental composition and the oxidation/reduction states in the first atomic layers of the palladium in the synthesized photocatalyst [39,40]. Quantitative XPS was carried out on the 0.25 wt% Pd-TiO_2 as follows: (a) before photoreduction; (b) after 60 min of near-UV photoreduction; and (c) after 24 h of near-UV photoreduction. It was observed that there was a significant increase in Pd^0: from 49.8% after photocatalyst synthesis to 81.7% after 1 h of near-UV irradiation, and up to close to 100% after 24 h under near-UV. Additional details regarding photocatalyst characterization can be found in Rusinque et al. [17,20,25,41].

4.3. Photo-CREC Water-II Reactor

The Photo-CREC Water-II (PCW-II) Reactor is an innovative photocatalytic slurry batch unit used for hydrogen production. It was developed at the CREC (Chemical Reactor Engineering Centre) at the University of Western Ontario. The unit is equipped, as shown in Figure 17, with the following components: (a) a tubular photocatalytic reactor equipped with two concentric tubes, a Pyrex glass inner tube and a near-UV opaque polyethylene outer tube; (b) a centrifugal pump; and (c) a hydrogen stirred storing/sealing tank. The light source (a near-UV lamp or, alternatively, a fluorescent visible light) is placed inside the transparent borosilicate glass tube. This Pyrex glass absorbs only 5% of the near-UV light emitted by the lamp [28]. The PCW-II reactor has a volume capacity of 6000 mL. The free-flowing slurry photocatalyst suspension circulates in the concentric annular space between the transparent Pyrex glass inner tube and the near-UV opaque polyethylene outer tube.

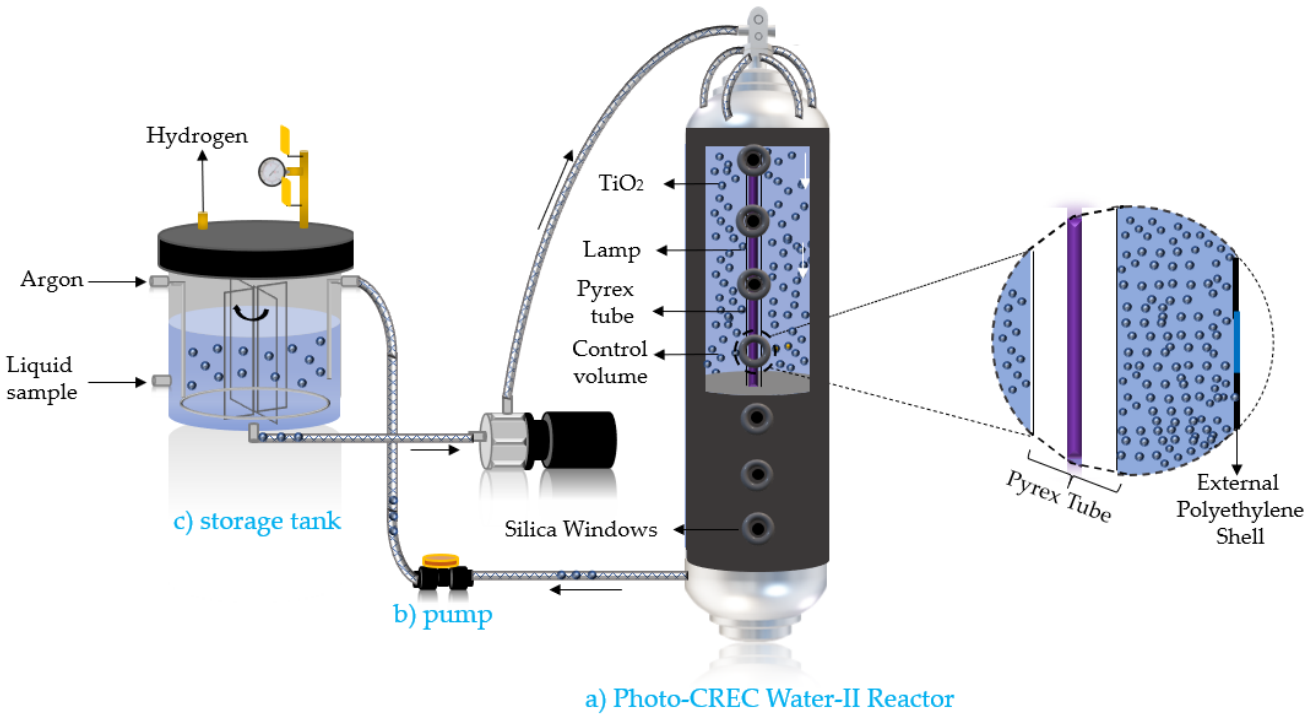


Figure 17. Schematic representation of the Photo-CREC Water-II Reactor: (**a**) tubular Photo-CREC Water-II Reactor with downflow slurry circulation; (**b**) centrifugal pump; and (**c**) sealed hydrogen storage tank.

For the photocatalytic water splitting reactions with near-UV light, a 15 W Ushio Black Light Blue lamp was used. This lamp has a detected output power of 1.61 W and emits, on average, 325.1 kJ/photon moles. The irradiation spectrum emitted is in the range of 340 nm

to 410 nm, with a maximum spectral peak identified at 368 nm [42]. On the other hand, for the visible light runs, a 15 W Philips mercury cool white lamp was used. The 1.48 W output power fluorescent lamp emits an average photon energy of 274.5 kJ/photon moles in the 300–700 nm range.

4.4. Photocatalytic Experiments

Photocatalytic experiments took place in the PCW-II reactor with a BLB near-UV lamp or, alternatively, with a fluorescent visible light lamp. The storage/mixing tank was initially loaded with 6000 mL of water and 2.0 v/v% of ethanol as a scavenger. The pH was adjusted at the beginning of the reaction to 4 ± 0.05, using H_2SO_4 [2 M]. The 0.25 wt% Pd-TiO_2 photocatalyst was sonicated for 10 min to ensure good particle distribution. Then, 0.15 g L^{-1} of the photocatalyst were added to the solution. The lamp was turned on for 30 min prior to the reaction to achieve lamp stabilization. The photocatalyst was sonicated for 10 min prior to its addition to the reactor, to ensure uniform particle distribution.

Once a uniform photocatalyst dispersion was achieved in the reactor, after turning on the pump, the mixing tank was sealed. Argon was used as an inert gas for oxygen removal, from the gas phase, in the hydrogen storage tank. Gas and liquid samples were taken every hour.

4.5. Analytical Techniques

A Shimadzu GC2010 Gas Chromatograph (Mandel, Guelf, ON, Canada) with argon (Praxair 99.999%) as a carrier gas was employed to analyze the gas phase chemical species. The Gas Chromatograph unit was equipped with a HayeSepD 100/120 mesh packed column (9.1 m × 2 mm × 2 μm nominal SS) (Sigma Aldrich, Oakville, ON, Canada) used for the separation of hydrogen from air. Additional details and information regarding the GC analysis of the Pd-TiO_2 photocatalyst are provided in Appendix D.

A Shimadzu HPLC Model UFLC (ultra-fast liquid chromatography) System was utilized, with 0.1% H_3PO_4 as a mobile phase, to analyze the liquid phase. The column used was the Supelcogel C-610H 30 cm × 7.8 mm ID. This quantitative analysis was performed by employing the RID (Refractive Index Detector) 10A, due to the polar nature of ethanol. The HPLC separated ethanol from water for further quantification.

Regarding the H_2O_2, the low concentrations (0–10 mg L^{-1}) were determined using a colorimetric method in conjunction with a spectrophotometer Spectronic 200+ from Thermo Spectronic (Thermo Fischer, Mississauga, ON, Canada). The H_2O_2 was detected with KI and N-dimethyl-p-phenylenediamine (DPD). The collected sample was mixed with ammonium molybdate, which decomposes the H_2O_2 and allows the KI to be oxidized to iodine [30]. The formed iodine oxidizes the DPD compound, generating a pink color. The pink color was then measured at 530 nm using a spectrophotometer (Spectronic 200+, Thermo Spectronic, which provides a 340 nm to 950 nm wavelength range and a nominal spectral bandwidth of 20 nm.

All the reagents used for hydrogen peroxide detection were purchased from Hach® (London, ON, Canada). A commercial H_2O_2 technical-grade solution (30% w/w of H_2O_2) was supplied by BioShop Canada (Burlington, ON, Canada).

The pH was measured with a digital pH meter Thermo Scientific Orion Star, with an accuracy of ±0.05. The pH was monitored in the slurry every hour, to determine its effect during the photocatalytic reaction.

5. Conclusions

(a) Suitable kinetics can be implemented for hydrogen production when using a mesoporous Pd-TiO_2 photocatalyst synthesized using a sol–gel method.
(b) The state of the added palladium as Pd^0 in the Pd-TiO_2 photocatalyst is critical to achieving high hydrogen formation rates.
(c) The proposed kinetics can be successfully evaluated in a Photo-CREC Water-II Reactor with controlled photon absorption rates.

(d) An "*in series-parallel*" reaction network is found to be suitable for the hydrogen formation kinetics when using a 0.25%wt Pd-TiO_2 photocatalyst.
(e) A best 34.8 $QY_{H^\bullet}$% can be obtained under near-UV light when employing a 0.25 wt% Pd-TiO_2 photocatalyst at a 1.00 g L^{-1} concentration.
(f) A best 8.80 $QY_{H^\bullet}$% can be achieved under visible light when using a 24 h near-UV photoreduced 0.25 wt% Pd-TiO_2 at a 0.15 g L^{-1} concentration.

Author Contributions: Conceptualization, investigation, writing, editing, reviewing final version of the original manuscript and supervision, H.d.L.; technical methodology, editing, reviewing final version of the original manuscript and co-supervision, S.E.; investigation, experimental methodology, reaction mechanism, kinetic model, formal analysis and writing original draft and final article, B.R. All authors have read and agreed to the published version of the manuscript.

Funding: This research was funded by the RGPIN-2021-03743 Natural Sciences and Engineering Research Council of Canada (NSERC) grant awarded to Hugo de Lasa.

Data Availability Statement: The data supporting this research is reported within the manuscript and the references given in the text.

Acknowledgments: We would like to thank Florencia de Lasa, who assisted with the editing of this paper and the 3D modeling of the graphical abstract.

Conflicts of Interest: The authors declare no conflict of interest.

Nomenclature

Ce	Concentration in the liquid of adsorbate at equilibrium
CO	Carbon monoxide
CO_2	Carbon dioxide
CH_4	Methane
C_2H_6	Ethane
C_2H_4	Ethylene
C_2H_4O	Acetaldehyde
D_p	Pore diameter (cm)
e^-	Electron
h+	Hole
F-127	Poly (ethylene oxide)/poly (propylene oxide)/poly (ethylene oxide)
$H^\bullet$	Hydrogen radical
H_2	Molecular Hydrogen
H_2O	Water
H_2O_2	Hydrogen Peroxide
K	Adsorption constant
L-H	Langmuir-Hinshelwood
n_m	Reaction rate order
OH^-	Hydroxide ions
$OH^\bullet$	Hydroxyl radical
Pd	Palladium
$PdCl_2$	Palladium II chloride
PEO	Poly (ethylene oxide)
PPO	Poly (propylene oxide)
Q_e	Equilibrium adsorbent-phase concentration
$Q_{e,max}$	Maximum adsorption capacity
t	Time (h)
TiO_2	Titanium dioxide

Acronyms

BLB	Black Light Blue Lamp
BET	Brunauer–Emmett–Teller Surface Area Method
DP25	Degussa P25 (TiO_2)
DPD	N, N-dimethyl-p-phenylenediamine
EISA	Evaporation-Induced-Self-Assembly
FID	Flame Ionization Detector
GC	Gas Chromatography
HPLC	High Performance Liquid Chromatography
LVRPA	Local Volumetric Rate of Photon Absorption
MIEB	Macroscopic Irradiation Energy Balance
PCW-II	Photo-CREC Water-II Reactor
pH	Potential of Hydrogen
$QY_{H^\bullet}$%	Quantum Yield based on $H^\bullet$ radicals formed
QY_{H2}%	Quantum Yields based on H_2 formed
STP	Standard Temperature and Pressure (273 K and 1 atm)
TPR	Temperature Programmed Reduction
TCD	Thermal Conductivity Detector
UV	Ultraviolet
VB	Valence Band
VIS	Visible light
XPS	X-ray Photoelectron Spectroscopy
XRD	X-ray Diffraction

Appendix A. Kinetic Modeling

Reaction rates for the formed oxidation by-products can be modeled as a function of the ethanol adsorbed species as follows:

$$r = k_i' \, K_j^A \, Q_{EtOH,max} \tag{A1}$$

1. For oxidation steps
   (a) Acetaldehyde (C_2H_4O)

$$C_2H_5OH + 2OH^\bullet \xrightarrow{k_2} C_2H_4O + 2H_2O$$

$$-r_{EtOH} = -\frac{1}{2} r_{OH^\bullet} = r_{C_2H_4O} = \frac{1}{2} r_{H_2O}$$

$$-r_{OH^\bullet} = 2\, r_{C_2H_4O}$$

$$-r_{OH^\bullet} = 2\, k_2 \, Q_{EtOH,max} \, Q_{OH^\bullet}^{n_1}$$

$$\boldsymbol{r_{C_2H_4O} = k_2 \, Q_{EtOH,max} \, Q_{OH^\bullet}^{n_1}} \tag{A2}$$

   (b) Carbon Dioxide (CO_2)

$$C_2H_5OH + 12OH^\bullet \xrightarrow{k_3} 2CO_2 + 9H_2$$

$$-r_{EtOH} = -\frac{1}{12} r_{OH^\bullet} = \frac{1}{2} r_{CO_2} = \frac{1}{9} r_{H_2O}$$

$$-r_{OH^\bullet} = 6\, r_{CO_2}$$

$$-r_{OH^\bullet} = 6\, k_3 \, Q_{EtOH,max} \, Q_{OH^\bullet}^{n_2}$$

$$\boldsymbol{r_{CO_2} = k_3 \, Q_{EtOH,max} \, Q_{OH^\bullet}^{n_2}} \tag{A3}$$

   (c) Hydrogen Peroxide (H_2O_2)

$$OH^\bullet + OH^\bullet \xrightarrow{k_4} H_2O_2$$

$$-\frac{1}{2}r_{OH\bullet} = r_{H_2O_2}$$
$$-r_{OH\bullet} = 2\,r_{H_2O_2}$$
$$-r_{OH\bullet} = 2\,k_4 Q_{OH\bullet}^3$$
$$\boldsymbol{r_{H_2O_2} = k_4 Q_{OH\bullet}^{n3}} \quad (A4)$$

(d) pH Variation

$$OH^\bullet \xrightarrow{k_5} e^- + OH^-$$
$$-r_{OH\bullet} = r_{OH^-}$$
$$-r_{OH\bullet} = k_5 Q_{OH\bullet}^4$$
$$\boldsymbol{r_{OH^-} = k_5 Q_{OH\bullet}^{n4}} \quad (A5)$$

(e) Hydroxyl Radical ($OH^\bullet$) Consumption—Formation

$$\boldsymbol{r_{OH\bullet} = k_1 - 2\,k_2\,Q_{EtOH,max}\,Q_{OH\bullet}^{n1} - 6\,k_3 Q_{EtOH,max}\,Q_{OH\bullet}^{n2} - 2\,k_4\,Q_{OH\bullet}^{n3} - k_5\,Q_{OH\bullet}^{n4}} \quad (A6)$$

By applying the steady state $\frac{dN_{OH\bullet}}{dt} = 0$ and the quasi-constant ethanol concentration approximations, this results in the following equation:

$$k_1 = 2\,k_2\,Q_{EtOH,max}\,Q_{OH\bullet}^{n1} + 6\,k_3 Q_{EtOH,max}\,Q_{OH\bullet}^{n2} + 2\,k_4\,Q_{OH\bullet}^{n3} + k_5\,Q_{OH\bullet}^{n4} \quad (A7)$$

Given that, from the $OH^\bullet$ radicals formed, only a fraction of them is consumed at any given irradiation time, at a steady state, the hydroxyl radical concentration can be considered close to constant ($Q_{OH\bullet} \cong constant$) and can be expressed as:

$$\boldsymbol{k_1 = 2\,k_2'\,Q_{EtOH,max} + 6\,k_3'\,Q_{EtOH,max} + 2\,k_4' + k_5'} \quad (A8)$$

with $k'i = ki\ Q_{OH\bullet}$.

Consider n_m as the reaction rate order for each by-product.

2. For reduction steps Reaction rates for the formed reduction steps can be modeled as a function of the $H^\bullet$ and ethanol adsorbed species as follows:

(a) Methane (CH_4)

$$C_2H_5OH + 4H^\bullet \xrightarrow{k_6} 2CH_4 + H_2O$$
$$-r_{EtOH} = -\frac{1}{4}r_{H\bullet} = \frac{1}{2}r_{CH_4} = r_{H_2O}$$
$$-r_{H\bullet} = 2r_{CH_4}$$
$$-r_{H\bullet} = 2\,k_6 Q_{EtOH,max}\,Q_{H\bullet}^{n5}$$
$$\boldsymbol{r_{CH_4} = k_6 Q_{EtOH,max}\,Q_{H\bullet}^{n5}} \quad (A9)$$

(b) Ethane (C_2H_6)

$$C_2H_5OH + 2H^\bullet \xrightarrow{k_7} C_2H_6 + H_2O$$
$$-r_{EtOH} = -\frac{1}{2}r_{H\bullet} = r_{C_2H_6} = r_{H_2O}$$
$$-r_{H\bullet} = 2r_{C_2H_6}$$
$$-r_{H\bullet} = 2\,k_7\,Q_{EtOH,max}\,Q_{H\bullet}^{n6}$$
$$\boldsymbol{r_{C_2H_6} = k_7\,Q_{EtOH,max}\,Q_{H\bullet}^{n6}} \quad (A10)$$

(c) Ethylene (C_2H_4)

$$C_2H_5OH \xrightarrow{k_8} C_2H_4 + H_2O$$

$$-r_{EtOH} = r_{C_2H_4} = r_{H_2O}$$
$$r_{C_2H_4} = k_8\, Q_{EtOH,max} \quad \text{(A11)}$$

(d) Hydrogen (H_2)

$$2H^{\bullet} \xrightarrow{k_9} H_2$$
$$-\frac{1}{2} r_{H\bullet} = r_{H_2}$$
$$-r_{H\bullet} = 2\, r_{H_2}$$
$$-r_{H\bullet} = 2\, k_9\, Q_{H\bullet}^{n7}$$
$$r_{H_2} = k_9\, Q_{H\bullet}^{n7} \quad \text{(A12)}$$

(e) H• Consumption—Formation

$$r_{H\bullet} = r_{H\bullet} - 2r_{CH_4} - 2r_{C_2H_6} - 2r_{H\bullet}$$

Considering that $r_{H\bullet} = r_{OH\bullet}$, then:

$$r_{H\bullet} = k_1 - 2\, k_6\, Q_{EtOH,max}\, Q_{H\bullet}^{n5} - 2\, k_7\, Q_{EtOH,max}\, Q_{H\bullet}^{n6} - 2\, k_9\, Q_{H\bullet}^{n7} \quad \text{(A13)}$$

By applying the steady-state approximation $\frac{dN_{H\bullet}}{dt} = 0$, and the ethanol concentration inequality, this results in Equation (A14):

$$k_1 = 2\, k_6\, Q_{EtOH,max}\, Q_{H\bullet}^{n5} + 2\, k_7\, Q_{EtOH,max}\, Q_{H\bullet}^{n6} + 2\, k_9\, Q_{H\bullet}^{n7} \quad \text{(A14)}$$

In addition, given that, at any given irradiation time, the H• radicals can be at a steady state, the hydroxyl radicals concentration is close to constant ($Q_{H\bullet} \cong constant$) and Equation (A14) can be expressed as:

$$k_1 = 2\, k_6{}'\, Q_{EtOH,max} + 2\, k_7{}'\, Q_{EtOH,max} + 2\, k_9{}' \quad \text{(A15)}$$

with $k'i = ki\, Q_H\bullet$.

Appendix B. Quantum Yield Calculation

The $QY_{H\bullet}\%$ can be defined as the number of moles of hydrogen radicals produced per absorbed photons on the photocatalyst surface.

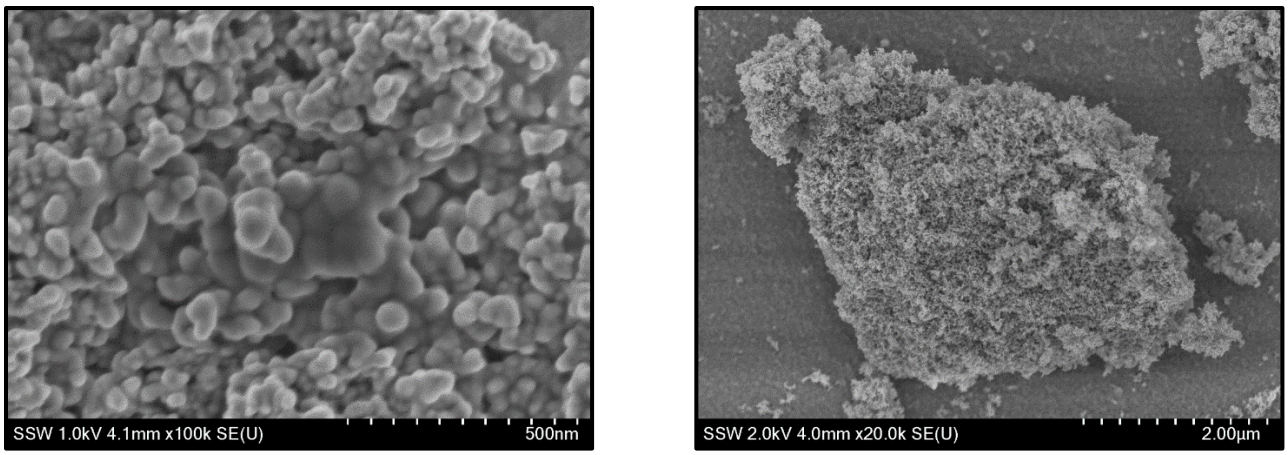
A sample $QY_{H\bullet}\%$ calculation given below considers a hydrogen production rate of 0.2159 μmol*cm^{-3} h^{-1}, using: (a) 0.25 wt.% Pd-TiO_2; (b) a photocatalyst concentration of 1.0 g L^{-1}; (c) ethanol at 2.0 v/v%; (d) initial pH = 4 ± 0.05; (e) near-UV light; (f) a gas phase volume in the reactor of 5716 cm^3, and (g) Pa = 1.97 × 10^{-6} Einstein s^{-1}.

$$QY_{H\bullet} = \frac{2 * \left(0.2159 \frac{\mu mol}{cm^3 h}\right) * \left(6.022 \times 10^{23} \frac{photon}{mol\ H_2}\right) * \left(\frac{1h}{3600\ s}\right)}{1.97 \times 10^{-6}\ Einsteins/s}$$
$$QY_{H\bullet} = 34.8\%$$

Appendix C. Scanning Electron Microscopy (SEM)

Scanning Electron Microscopy (SEM) provides detailed high-resolution images of the 0.25 wt% Pd-TiO_2 photocatalyst.

The semiconductor material was analyzed by scanning electron microscopy using a Hitachi SU8230 Regulus ultra-high resolution field emission scanning electron microscope (FESEM). SEM imaging was performed using accelerating voltages ranging from 1 to 2 kV, as observed in Figure A1.



(**a**) (**b**)

Figure A1. Scan Electron Microscope images for the 0.25 wt% Pd-TiO_2 photocatalyst at two different accelerating voltages: (**a**) 1.0 kV; and (**b**) 2.0 kV.

Appendix D. Detection of H_2 and Carbon Containing Species by a Shimadzu CG 2010

The several gases produced from the photocatalytic water splitting reaction with ethanol as a scavenger were quantified using a Shimadzu GC2010 Gas Chromatograph (Nakagyo-ku, Kyoto, Japan). Samples were taken every hour.

To accomplish this, argon (Praxair 99.999%) was used as a gas carrier. The GC was equipped with two detectors: a Flame Ionization Detector (Nakagyo-ku, Kyoto, Japan) (FID) coupled with a Methanizer and a Thermal Conductivity Detector (TCD). As a result, the analytical equipment employed was able to detect hydrogen (H_2), carbon monoxide (CO), methane (CH_4), carbon dioxide (CO_2), ethane (C_2H_6), ethylene (C_2H_4), acetaldehyde (C_2H_4O) and ethanol (C_2H_5OH).

The GC method used for the gas phase analysis is described as follows:

Column:

Temperature: 50 °C, equilibration time: 0.2 min

Table A1. Column Oven Temperature Program.

Rate	Temperature (°C)	Hold Time (min)
-	50	4
20.0	200	18.5

FID:

Temperature: 230 °C, sample rate: 40 ms, make up gas: hydrogen

TCD:

Temperature: 210 °C, sample rate: 40 ms, make up gas: argon

Typical chromatograms obtained for hydrogen and carbon-containing by-products using the employed programmed oven temperature method are reported in Figures A2 and A3. Air detected via the TCD was attributed to the air contained in the needle when injecting the gas sample into the GC. This air gas volume is negligible and was disregarded in the product analysis.

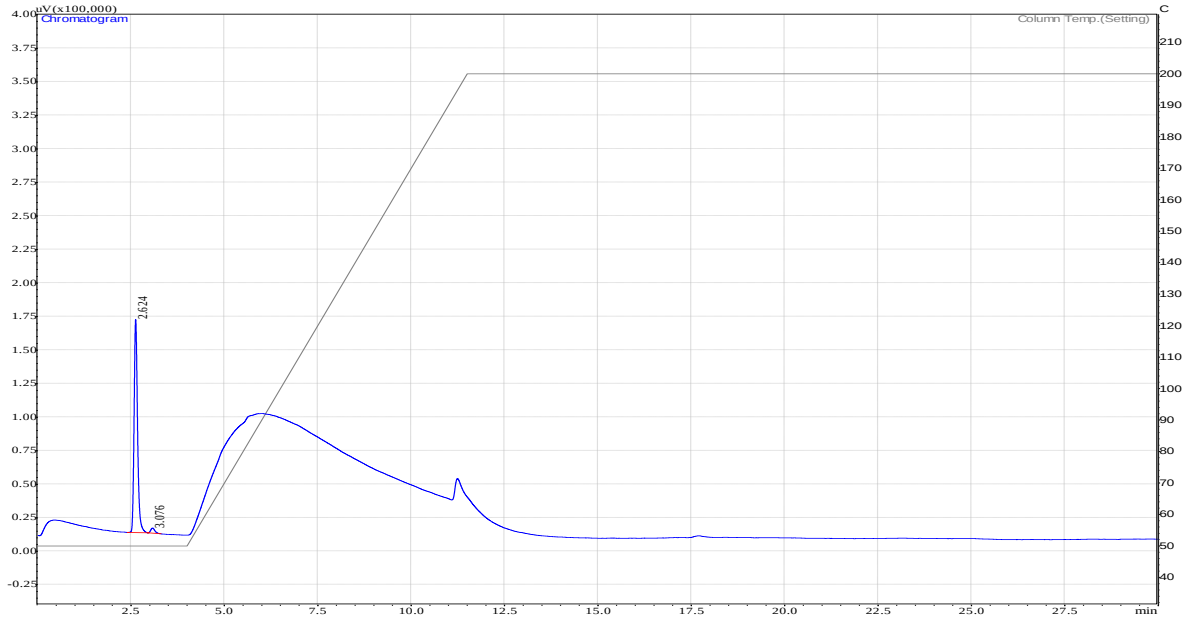


Figure A2. Hydrogen peak as detected by the TCD.

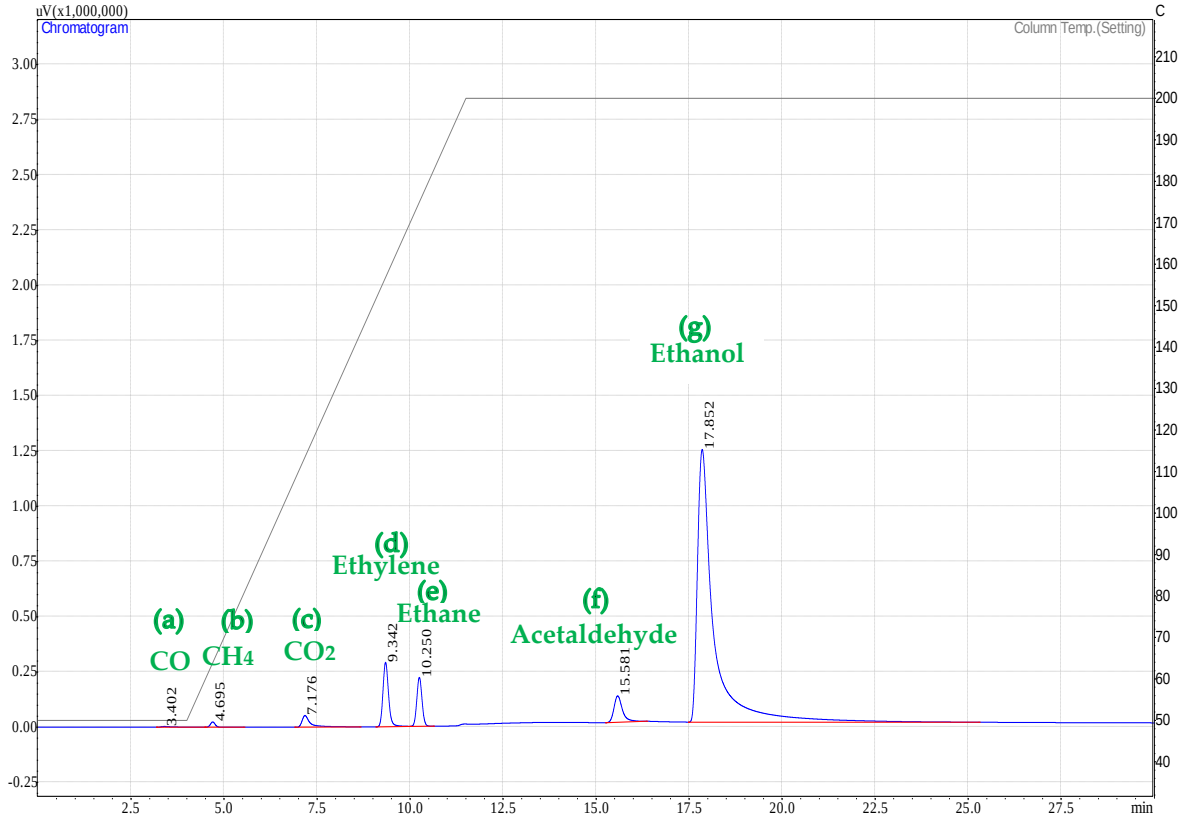


Figure A3. Carbon containing product species peaks as detected by the FID for: (a) carbon monoxide (CO); (b) methane (CH_4); (c) carbon dioxide (CO_2); (d) ethylene (C_2H_4); (e) ethane (C_2H_6); (f) acetaldehyde (C_2H_4O); and (g) ethanol (C_2H_5OH).

The H_2 gas chromatographic peaks were quantified using the TCD calibration, as reported in Figure A4. Calibration was established by using an H_2 certified standard gas mixture sample (10% H_2 and 90% He Praxair) and different hydrogen volumes (0.1, 0.2, 0.3,

0.4, 0.5 and 0.6 mL). Injected sample gas volumes were at room temperature and standard pressure conditions (25 °C and 1 atm).

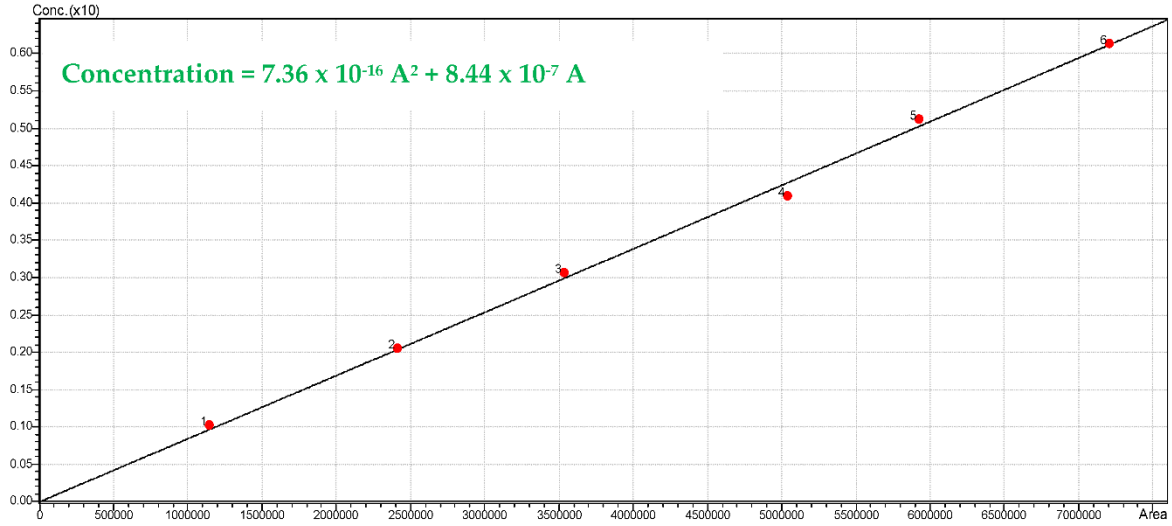


Figure A4. Calibration curve using the Shimadzu GC 2010 for hydrogen.

References

1. Chang, T.; Chu, H.-P.; Chen, W.-Y. Energy consumption and economic growth in 12 Asian countries: Panel data analysis. *Appl. Econ. Lett.* **2013**, *20*, 282–287. [CrossRef]
2. Maeda, K.; Teramura, K.; Lu, D.; Takata, T.; Saito, N.; Inoue, Y.; Domen, K. Photocatalyst releasing hydrogen from water. *Nature* **2006**, *440*, 295. [CrossRef] [PubMed]
3. Khan, M.M.; Adil, S.; Al-Mayouf, A. Metal oxides as photocatalysts. *J. Saudi Chem. Soc.* **2015**, *19*, 462–464. [CrossRef]
4. Holloway, P.H.; McGuire, G.E. *Handbook of Compound Semiconductor*; Noyes Publications: Norwich, NJ, USA, 1995.
5. Haider, A.J.; Anbari, R.H.A.; Kadhim, G.R.; Salame, C.-T. Exploring potential Environmental applications of TiO_2 Nanoparticles. *Energy Procedia* **2017**, *119*, 332–345. [CrossRef]
6. Lee, S.-Y.; Park, S.-J. TiO_2 photocatalyst for water treatment applications. *J. Ind. Eng. Chem.* **2013**, *19*, 1761–1769. [CrossRef]
7. Change, C. Global Warming: A public health crisis demanding inmediate action. *World Aff. Summer* **2007**, *11*, 44–58.
8. Chen, X.; Shen, S.; Guo, L.; Mao, S.S. Semiconductor-based Photocatalytic Hydrogen Generation. *Chem. Rev.* **2010**, *110*, 6503–6570. [CrossRef] [PubMed]
9. Acar, C.; Dincer, I.; Naterer, G. Review of photocatalytic water-splitting methods for sustainable hydrogen production. *Int. J. Energy Res.* **2016**, *40*, 1449–1473. [CrossRef]
10. Cushing, S.; Li, J.; Meng, F.; Senty, T.R.; Suri, S.; Zhi, M.; Li, M.; Bristow, A.D.; Wu, N. Photocatalytic Activity Enhanced by Plasmonic Resonant Energy Transfer from Metal to Semiconductor. *J. Am. Chem. Soc.* **2012**, *134*, 15033–15041. [CrossRef]
11. Yang, J.; Wang, D.; Han, H.; Li, C. Roles of Cocatalysts in Photocatalysis and Photoelectrocatalysis. *Acc. Chem. Res.* **2013**, *46*, 1900–1909. [CrossRef]
12. Etacheri, V.; Di Valentin, C.; Schneider, J.; Bahnemann, D.B.D.; Pillai, S.C. Visible-light activation of TiO_2 photocatalysts: Advances in theory and experiments. *J. Photochem. Photobiol. C Photochem. Rev.* **2015**, *25*, 1–29. [CrossRef]
13. Nguyen, V.-H.; Wu, J.C. Recent developments in the design of photoreactors for solar energy conversion from water splitting and CO_2 reduction. *Appl. Catal. A Gen.* **2018**, *550*, 122–141. [CrossRef]
14. Wang, M.; Shen, S.; Li, L.; Tang, Z.; Yang, J. Effects of sacrificial reagents on photocatalytic hydrogen evolution over different photocatalysts. *J. Mater. Sci.* **2017**, *52*, 5155–5164. [CrossRef]
15. López, C.R.; Melián, E.P.; Méndez, J.O.; Santiago, D.E.; Rodríguez, J.D.; Díaz, O.G. Comparative study of alcohols as sacrificial agents in H2production by heterogeneous photocatalysis using Pt/TiO_2 catalysts. *J. Photochem. Photobiol. A Chem.* **2015**, *312*, 45–54. [CrossRef]
16. Escobedo, S. Photocatalytic Water Splitting Using a Modified Pt- TiO_2. Kinetic Modeling and Hydrogen Production Efficiency. Ph.D. Thesis, The University of Western Ontario, London, ON, Canada, 2013.
17. Rusinque, B.; Escobedo, S.; De Lasa, H. Photoreduction of a Pd-Doped Mesoporous TiO_2 Photocatalyst for Hydrogen Production under Visible Light. *Catalysts* **2020**, *10*, 74. [CrossRef]
18. Thornton, J.M.; Raftery, D. Efficient Photocatalytic Hydrogen Production by Platinum-Loaded Carbon-Doped Cadmium Indate Nanoparticles. *ACS Appl. Mater. Interfaces* **2012**, *4*, 2426–2431. [CrossRef]
19. Maicu, M.; Hidalgo, M.C.; Colón, G.; Navío, J.A. Comparative study of the photodeposition of Pt, Au and Pd on pre-sulphated TiO_2 for the photocatalytic decomposition of phenol. *J. Photochem. Photobiol. A Chem.* **2011**, *217*, 275–283. [CrossRef]

20. Rusinque, B.; Escobedo, S.; De Lasa, H. Photocatalytic Hydrogen Production Under Near-UV Using Pd-Doped Mesoporous TiO_2 and Ethanol as Organic Scavenger. *Catalysts* **2019**, *9*, 33. [CrossRef]
21. Rusinque, B.; Escobedo, S.; de Lasa, H. Hydrogen Production via Pd-TiO_2 Photocatalytic Water Reaction Mechanism. *Catalysts* **2021**, *11*, 405. [CrossRef]
22. Tambago, H.M.G.; de Leon, R.L. Intrinsic Kinetic Modeling of Hydrogen Production by Photocatalytic Water Splitting Using Cadmium Zinc Sulfide Catalyst. *Int. J. Chem. Eng. Appl.* **2015**, *6*, 220–227. [CrossRef]
23. Liu, L.; Luo, X.-B.; Deng, L.; Luo, S.-L. Application of Nanotechnology in the Removal of Heavy Metal From Water. In *Nanomaterials for the Removal of Pollutants and Resource Reutilization*; Elsevier: Amsterdam, The Netherlands, 2019; pp. 83–147.
24. Escobedo, S.; Serrano, B.; Calzada, A.; Moreira, J.; de Lasa, H. Hydrogen production using a platinum modified TiO_2 photocatalyst and an organic scavenger. Kinetic modeling. *Fuel* **2016**, *181*, 438–449. [CrossRef]
25. Rusinque, B. Hydrogen Production by Photocatalytic Water Splitting Under Near-UV and Visible Light Using Doped Pt and Pd TiO_2. Ph.D. Thesis, The University of Western Ontario, London, ON, Canada, August 2021.
26. Ibrahim, H.; de Lasa, H. Novel Photocatalytic Reactor for the Destruction of Airborne Pollutants Reaction Kinetics and Quantum Yields. *Ind. Eng. Chem. Res.* **1999**, *38*, 3211–3217. [CrossRef]
27. Escobedo, S.; Rusinque, B.; de Lasa, H. Photochemical Thermodynamic Efficiency Factors (PTEFs) for Hydrogen Production Using Different TiO_2 Photocatalysts. *Ind. Eng. Chem. Res.* **2019**, *58*, 22225–22235. [CrossRef]
28. de Lasa, H.; Serrano, B.; Salaices, M. Photocatalytic Reaction Engineering. In *Photocatalytic Reaction Engineering*; Springer: New York, NY, USA, 2005.
29. Salas, S.E.; Rosales, B.S.; de Lasa, H. Quantum yield with platinum modified TiO_2 photocatalyst for hydrogen production. *Appl. Catal. B Environ.* **2013**, *140–141*, 523–536. [CrossRef]
30. Ravishankar, T.N.; Vaz, M.D.O.; Ramakrishnappa, T.; Teixeira, S.R.; Dupont, J.; Pai, R.K.; Banuprakash, G. The heterojunction effect of Pd on TiO_2 for visible light photocatalytic hydrogen generation via water splitting reaction and photodecolorization of trypan blue dye. *J. Mater. Sci. Mater. Electron.* **2018**, *29*, 11132–11143. [CrossRef]
31. Guayaquil-Sosa, J.; Rosales, B.S.; Valadés-Pelayo, P.; De Lasa, H. Photocatalytic hydrogen production using mesoporous TiO_2 doped with Pt. *Appl. Catal. B Environ.* **2017**, *211*, 337–348. [CrossRef]
32. Das, S.K.; Bhunia, M.K.; Bhaumik, A. Self-assembled TiO_2 nanoparticles: Mesoporosity, optical and catalytic properties. *Dalton Trans.* **2010**, *39*, 4382–4390. [CrossRef] [PubMed]
33. Rusinque, B. Hydrogen Production by Photocatalytic Water Splitting under Near-UV using Pd doped Mesoporous TiO_2. In Proceedings of the Nam 26. 2019 North American Catalysis Society Meeting, Chicago, IL, USA, 23–28 June 2019.
34. Deshmane, V.; Owen, S.L.; Abrokwah, R.Y.; Kuila, D. Mesoporous nanocrystalline TiO_2 supported metal (Cu, Co, Ni, Pd, Zn, and Sn) catalysts: Effect of metal-support interactions on steam reforming of methanol. *J. Mol. Catal. A Chem.* **2015**, *408*, 202–213. [CrossRef]
35. Alencar, C.S.L.; Paiva, A.R.N.; Da Silva, J.C.M.; Vaz, J.M.; Spinacé, E.V. One-Step Synthesis of AuCu/TiO_2 Catalysts for CO Preferential Oxidation. *Mater. Res.* **2020**, *23*, 2–7. [CrossRef]
36. Bratan, V.; Munteanu, C.; Hornoiu, C.; Vasile, A.; Papa, F.; State, R.; Preda, S.; Culita, D.; Ionescu, N. CO oxidation over Pd supported catalysts—In situ study of the electric and catalytic properties. *Appl. Catal. B Environ.* **2017**, *207*, 166–173. [CrossRef]
37. Micromeritics. *AutoChem 2920 Automated Catalyst Characterization System Operator's Manual*; Norcross, GA, USA, 2014. Available online: https://www.google.com.hk/url?sa=t&rct=j&q=&esrc=s&source=web&cd=&ved=2ahUKEwieg93lhLv1AhXWMd4KHU2lAQkQFnoECAcQAQ&url=https%3A%2F%2Fwww.micromeritics.com%2FRepository%2FFiles%2FAutoChem_II_2920_Operator_Manual_V4.00.pdf&usg=AOvVaw3PJqZ-QHngNh9zjwIXSemb (accessed on 28 December 2021).
38. Sobana, N.; Muruganadham, M.; Swaminathan, M. Nano-Ag particles doped TiO_2 for efficient photodegradation of Direct azo dyes. *J. Mol. Catal. A Chem.* **2006**, *258*, 124–132. [CrossRef]
39. Briggs, D. X: X-ray Photoelectron Spectroscopy. In *Handbook of Adhesion*, 2nd ed.; Wiley: Hoboken, NJ, USA, 2005; pp. 621–622.
40. Lee, J.; Choi, W. Photocatalytic Reactivity of Surface Platinized TiO_2: Substrate Specificity and the Effect of Pt Oxidation State. *J. Phys. Chem. B* **2005**, *109*, 7399–7406. [CrossRef] [PubMed]
41. Rusinque, B. Hydrogen Production by Photocatalytic Water Splitting Under Near-UV and Visible Light Using Doped Pt and Pd TiO_2. Master's Thesis, The University of Western Ontario, London, ON, Canada, September 2018.
42. Ushio. *Uv-b, bl & blb. Catalog 2016*; Ushio: Cypress, CA, USA, 2016.